NAVAL POSTGRADUATE SCHOOL

MONTEREY, CALIFORNIA

THESIS

AN ANALYSIS OF THE USE OF A LEAD-COOLED FAST REACTOR FOR HYDROGEN PRODUCTION IN AN EABO ENVIRONMENT

by

Weston Patrick

June 2022

Thesis Advisor:	Craig F. Smith
Co-Advisor:	Eric Hahn
Second Reader:	Alan R. Howard

THIS PAGE INTENTIONALLY LEFT BLANK

REPORT DOCUMENTATION PAGE	*Form Approved OMB No. 0704-0188*

1. AGENCY USE ONLY *(Leave blank)*	**2. REPORT DATE** June 2022	**3. REPORT TYPE AND DATES COVERED** Master's thesis

4. TITLE AND SUBTITLE AN ANALYSIS OF THE USE OF A LEAD-COOLED FAST REACTOR FOR HYDROGEN PRODUCTION IN AN EABO ENVIRONMENT	**5. FUNDING NUMBERS**
6. AUTHOR(S) Weston Patrick	
7. PERFORMING ORGANIZATION NAME(S) AND ADDRESS(ES) Naval Postgraduate School Monterey, CA 93943-5000	**8. PERFORMING ORGANIZATION REPORT NUMBER**
9. SPONSORING / MONITORING AGENCY NAME(S) AND ADDRESS(ES) N/A	**10. SPONSORING / MONITORING AGENCY REPORT NUMBER**

11. SUPPLEMENTARY NOTES The views expressed in this thesis are those of the author and do not reflect the official policy or position of the Department of Defense or the U.S. Government.

12a. DISTRIBUTION / AVAILABILITY STATEMENT Approved for public release. Distribution is unlimited.	**12b. DISTRIBUTION CODE** A

13. ABSTRACT (maximum 200 words)

Expeditionary Advanced Base Operations (EABO) will require significant coordination across multiple branches to ensure sufficient sustainment capabilities, especially to meet the high energy demands for these operations. One solution to meet the extraordinary energy demands of EABO is through hydrogen production with a small modularized, lead-cooled fast reactor (LFR). Hydrogen could then be used as feedstock to produce synthetic hydrocarbons that could supplement conventional fuel through a Fischer-Tropsch process.

This thesis explores the various hydrogen production methods compatible with an LFR in an EABO environment. An analysis was conducted for each method to determine the most efficient operating conditions based on the typical operating ranges of a reference LFR. This analysis determined that a Hybrid Thermochemical Electrolysis process was the most effective method for hydrogen production when paired with an LFR and using a Supercritical Carbon Dioxide (S-CO2) Brayton cycle for energy conversion. It was also realized that the lack of testing performed with hybrid processes makes the feasibility of this technology being implemented promptly less likely. However, polymer electrolyte membrane (PEM) electrolysis was also found to be a very effective hydrogen production method and is a mature technology with commercially available options already existent that could meet the U.S.'s needs.

14. SUBJECT TERMS Fischer-Tropsch, FT, nuclear power, synthetic fuel, nuclear hydrogen production, small modular reactor, SMR, lead-cooled fast reactor, LFR, expeditionary advanced base operations, EABO, polymer electrolyte membrane, PEM	**15. NUMBER OF PAGES** 103
	16. PRICE CODE

17. SECURITY CLASSIFICATION OF REPORT	**18. SECURITY CLASSIFICATION OF THIS PAGE**	**19. SECURITY CLASSIFICATION OF ABSTRACT**	**20. LIMITATION OF ABSTRACT**
Unclassified	Unclassified	Unclassified	UU

NSN 7540-01-280-5500

Standard Form 298 (Rev. 2-89)
Prescribed by ANSI Std. 239-18

THIS PAGE INTENTIONALLY LEFT BLANK

Approved for public release. Distribution is unlimited.

AN ANALYSIS OF THE USE OF A LEAD-COOLED FAST REACTOR FOR HYDROGEN PRODUCTION IN AN EABO ENVIRONMENT

Weston Patrick
Lieutenant, United States Navy
BS, Northwest Nazarene University, 2013

Submitted in partial fulfillment of the
requirements for the degree of

MASTER OF SCIENCE IN APPLIED PHYSICS

from the

NAVAL POSTGRADUATE SCHOOL
June 2022

Approved by: Craig F. Smith
Advisor

Eric Hahn
Co-Advisor

Alan R. Howard
Second Reader

Joseph P. Hooper
Chair, Department of Physics

THIS PAGE INTENTIONALLY LEFT BLANK

ABSTRACT

Expeditionary Advanced Base Operations (EABO) will require significant coordination across multiple branches to ensure sufficient sustainment capabilities, especially to meet the high energy demands for these operations. One solution to meet the extraordinary energy demands of EABO is through hydrogen production with a small modularized, lead-cooled fast reactor (LFR). Hydrogen could then be used as feedstock to produce synthetic hydrocarbons that could supplement conventional fuel through a Fischer-Tropsch process.

This thesis explores the various hydrogen production methods compatible with an LFR in an EABO environment. An analysis was conducted for each method to determine the most efficient operating conditions based on the typical operating ranges of a reference LFR. This analysis determined that a Hybrid Thermochemical Electrolysis process was the most effective method for hydrogen production when paired with an LFR and using a Supercritical Carbon Dioxide (S-CO2) Brayton cycle for energy conversion. It was also realized that the lack of testing performed with hybrid processes makes the feasibility of this technology being implemented promptly less likely. However, polymer electrolyte membrane (PEM) electrolysis was also found to be a very effective hydrogen production method and is a mature technology with commercially available options already existent that could meet the U.S.'s needs.

THIS PAGE INTENTIONALLY LEFT BLANK

TABLE OF CONTENTS

LIST OF FIGURES

LIST OF TABLES

THIS PAGE INTENTIONALLY LEFT BLANK

LIST OF ACRONYMS, ABBREVIATIONS, AND SYMBOLS

ACRONYMS/ABBREVIATIONS

EABO	Expeditionary Advanced Base Operations
DI	De-ionized
FT	Fischer-Tropsch
GIF	Generation IV International Forum
HHV	Higher Heating Value
HTSE	High-Temperature Steam Electrolysis
LBE	Lead and Bismuth Eutectic Mixture
LFR	Lead Cooled Fast Reactor
LHV	Lower Heating Value
LWR	Light-water Reactor
NATO	North Atlantic Treaty Organization
OER	Oxygen Evolution Reaction.
PEM	Polymer Electrolyte Membrane
R&D	Research and Development
S-CO_2	Supercritical Carbon Dioxide
SLOC	Sea Lines of Communications
SMR	Small Modular Reactor
SOEC	Solid-Oxide Electrolyzer Cell
SSTAR	Small Secure Transportable Autonomous Reactor
STP	Standard Temperature and Pressure
WEZ	Weapon Engagement Zone

SYMBOLS

$\dot{V}_{H_2}$	Hydrogen Production Rate (Nm^3/hr)
η	Efficiency
η_F	Faradaic Efficiency
V_{mol}	Molar volume for a gas at STP (24.465×10^{-3} Nm^3)
F	Faraday's Constant (9.6485×10^4 C mol^{-1})

R	Gas Constant (8.314 J mol^{-1} K^{-1})
I	Current density (A cm^{-2})
ΔH_{HHV}	Higher Heating Value (J mol^{-1})
$\Delta_f H$	Enthalpy of formation (J mol^{-1})
$\Delta_f G$	Gibb's free energy of formation (J mol^{-1})
$\Delta_f Q$	Thermal energy of formation (J mol^{-1})
$\Delta_f S$	Entropy of formation (J $°K^{-1}$ mol^{-1})
T	temperature (°K/°C)
Q	Heating inputs (J)
Q_{HL}	Heat Loss (J)
W	Work inputs (J)
V	Voltage (Volts)
P	Power (W)
n_c	# of cells in series
z	# of electrons

SUBSCRIPTS

$comp$	Compressor
e	Energy
EC	Energy Conversion
HL	From heat loss
in	Input into system
$irrev$	Irreversible
$loss$	Irrecoverable
out	Output from system
OCV	Open circuit voltage
rev	Reversible
t	Turbine
TN	Thermoneutral
WS	Water splitting reaction

EXECUTIVE SUMMARY

With the return of the Great Power Competition, the U.S. must shift its focus to new threats posed by major competitors like China and Russia [1]. As part of this focus, the U.S. will require a well-developed plan for Expeditionary Advanced Base Operations (EABO). EABO will require significant joint and multinational coordination, especially to meet the high energy demands for these operations [2]. One technical approach that could contribute to the challenge of meeting the extraordinary energy demands of EABO is hydrogen production using a small modular, lead-cooled fast reactor (LFR). Hydrogen could then be used as feedstock to produce synthetic hydrocarbons that could supplement conventional fuel through a Fischer-Tropsch process.

This thesis explores the various hydrogen production methods compatible with an LFR in an EABO environment. These methods include Alkaline Water Electrolysis (AWE), Polymer Electrolyte Membrane (PEM) Electrolysis, High-Temperature Steam Electrolysis (HTSE), and Hybrid Thermochemical Electrolysis. A synopsis of each method provides advantages and disadvantages, and a review of LFR technology and Supercritical Carbon Dioxide (S-CO_2) Brayton energy conversion cycle is also provided.

An energy balance was conducted for each method to determine how the production efficiency would change based on the operating characteristics of a reference LFR to determine the most efficient production method. This analysis included calculating the change in electrolysis cell voltage, current, and efficiency with changes in cell operating temperatures. Because the hydrogen production rate is directly proportional to the cell's current, the power required for a given production value and range of operating temperatures could be determined [3], [4].

This analysis determined that a Hybrid Thermochemical Electrolysis process was the most effective method for hydrogen production when paired with an LFR and using an S-CO_2 Brayton cycle for energy conversion. It was also realized that the lack of testing performed with hybrid processes makes the feasibility of this technology being implemented promptly less likely. However, polymer electrolyte membrane (PEM)

electrolysis was also a very effective hydrogen production method and is a mature technology with commercially available options that could meet the U.S.'s needs.

References

[1] R. O'Rourke, "Renewed Great Power Competition: Implications for Defense," 10 March 2022. [Online]. Available: https://crsreports.congress.gov/product/pdf/R/R43838. [Accessed 1st April 2022].

[2] Department of the Navy, "Tentative Manual For Expeditionary Advanced Base Operations," February 2021. [Online]. Available: https://www.mcwl.marines.mil/TMEABO/

[3] A. Godula-Jopek, *Hydrogen Production: By Electrolysis*, Weinheim, Germany: John Wiley & Sons, Incorporated, 2015. [Online]. Available: ProQuest

[4] C. Lamy and P. Millet, "A critical review on the definition used to calculate the energy efficiency coefficients of water electrolysis cells working under near ambient temperature conditions," *Journal of Power Sources,* vol. 447, p. 227350, 2020. [Online]. Available: https://doi.org/10.1016/j.jpowsour.2019.227350

ACKNOWLEDGMENTS

Firstly, I would like to thank my thesis advisors, Dr. Craig Smith and Mr. Eric Hahn, for their incredible support and guidance in completing my thesis work.

Thank you to those who helped support me throughout my time at Naval Postgraduate School, my partner John Bunn, and my supporting friends, Adam Dickson, Cole Staudt, Tamer Kawas, and Benjamen Schierman.

THIS PAGE INTENTIONALLY LEFT BLANK

I. INTRODUCTION

With the reemergence of the Great Power Competition, the United States is seeing a dramatic shift in its national security priorities from the previous decades centered around counterterrorism. China and Russia have become increasingly more assertive. China's increased pressure and rhetoric to reunify with Taiwan and Russia's horrific invasion of Ukraine highlight this fact. These actions pose a significant threat to global U.S. interests. They have renewed discussions about the global presence and capability of the U.S. Military to deter and respond to aggressive actions by their competitors [1].

A significant component of this presence would be the U.S.'s capability to employ Expeditionary Advanced Base Operations (EABO). These operations are intended to counter the stand-off engagement capabilities of our global competitors by using expeditionary forces in a contested area to achieve air superiority, sea control, and assured communications. Maneuverability, resilience, and sustainability are all paramount for successful EABOs, but one of the most significant challenges to achieving these features is meeting the energy demands for these operations. Notably, conventional manned air assets will require considerable energy resources with minimal aggregate forces inside the adversary's weapon engagement zone (WEZ). Additionally, for any advanced bases to be self-sufficient, resilient, and efficient electric energy generation will be required. These energy requirements introduced a significant vulnerability in EABO to attacks on fuel supplies [2] and were even highlighted by ADM Richardson as an essential component to maritime superiority [3].

A potential option for supplying the requisite fuel to meet the energy demands of EABO is through synthetic fuel production using a Fischer-Tropsch (FT) method. This method uses a catalyst in an endothermic reaction to convert hydrogen and carbon-monoxide gas feedstock into hydrocarbon chains used for fuel [4], [5]. The resultant fuel is a cleaner fuel free of aromatics and Sulfur [6]. FT generators are not new, and their science is well established. The current climate crisis has also helped drive continued research and development in searching for alternative energy sources. The U.S. Naval Research Laboratory is also conducting ongoing research intending to develop a scalable

FT process that can be employed in an operational environment to supplement conventional fossil fuels [7]. Such a process would require a reliable energy source and abundant means of procuring the needed hydrogen and carbon-monoxide feedstock [7].

Beyond its use as a feedstock for synthetic fuel production, hydrogen can also function as means of energy storage. Using energy from such sources as wind, solar, or nuclear power into stores of hydrogen gas can then be used later through direct consumption (combustion or fuel cells) or as an FT feedstock [8]. Hydrogen is a long-term energy storage solution that will not degrade over time and is more resistant to environmental effects than batteries typically used [9]. These factors make hydrogen an excellent means of energy storage for EABO and other forward-deployed environments.

Nuclear power has long been considered one of the most efficient means of producing Energy. The U.S. Navy already has a long history of safe operation in powering their entire submarine and aircraft carrier fleets. In 2000, the Generation IV International (Gen-IV) Forum was established as a multinational collaboration effort to identify and develop the next generation of nuclear technology and shift the safety paradigm from risk mitigation to risk elimination through passive safety systems [10]. A Lead Cooled Fast Reactor (LFR) is one of the designs identified by the Gen-IV forum as having the potential to meet this initiative. It was identified as having the most significant potential for use in a remote location due to its sustainability through a closed fuel cycle, resistance to proliferation, and safety of its inert coolant [11]. For these reasons, an LFR would be well suited to meet the energy needs of hydrogen production for use in EABO and other forward-deployed operations.

A. OBJECTIVE

Providing reliable, efficient energy and abundant hydrogen production for EABO is a significant technical challenge. This thesis aims to analyze the use of an LFR to help meet the energy needs of EABO operations through efficient hydrogen production. It analyzes the various hydrogen production methods suited for an EABO environment to determine how the efficiency of these methods would be affected by using an LFR to power the processes. This analysis assesses which method is best suited for application to EABO

hydrogen production and will provide a technical approach to helping meet EABO energy needs following further research and development.

B. ORGANIZATION OF THESIS

This thesis is organized into six chapters. Chapter II presents an overview of hydrogen production methods suitable for use in an EABO environment. Chapter III provides an overview of how Lead Cooled Fast reactors work and a synopsis of the Small Secure Transportable Autonomous Reactor (SSTAR) used as the reference system for analysis. Chapter IV details the methodology used to analyze the efficiency of the different hydrogen production methods. Chapter V provides the analysis results and an assessment of which method is best suited for application in EABO. Chapter VI draws conclusions and recommendations for future research and development to meet the EABO energy needs.

THIS PAGE INTENTIONALLY LEFT BLANK

II. HYDROGEN PRODUCTION

Hydrogen is a versatile fuel and means of energy storage. It can produce electricity directly using a fuel cell or combustion engine [8]. It can also be used as a feedstock to produce synthetic fuel when combined with carbon monoxide through a Fischer Tropsch process [6]. Hydrogen can also function as means of energy storage by converting energy from such sources as wind, solar, or nuclear power into hydrogen stores through various processes that can be used at a needed time to convert back to electricity [8]. Figure 1 demonstrates how hydrogen can function as energy storage and transfer from production to distribution and ultimately end-use.

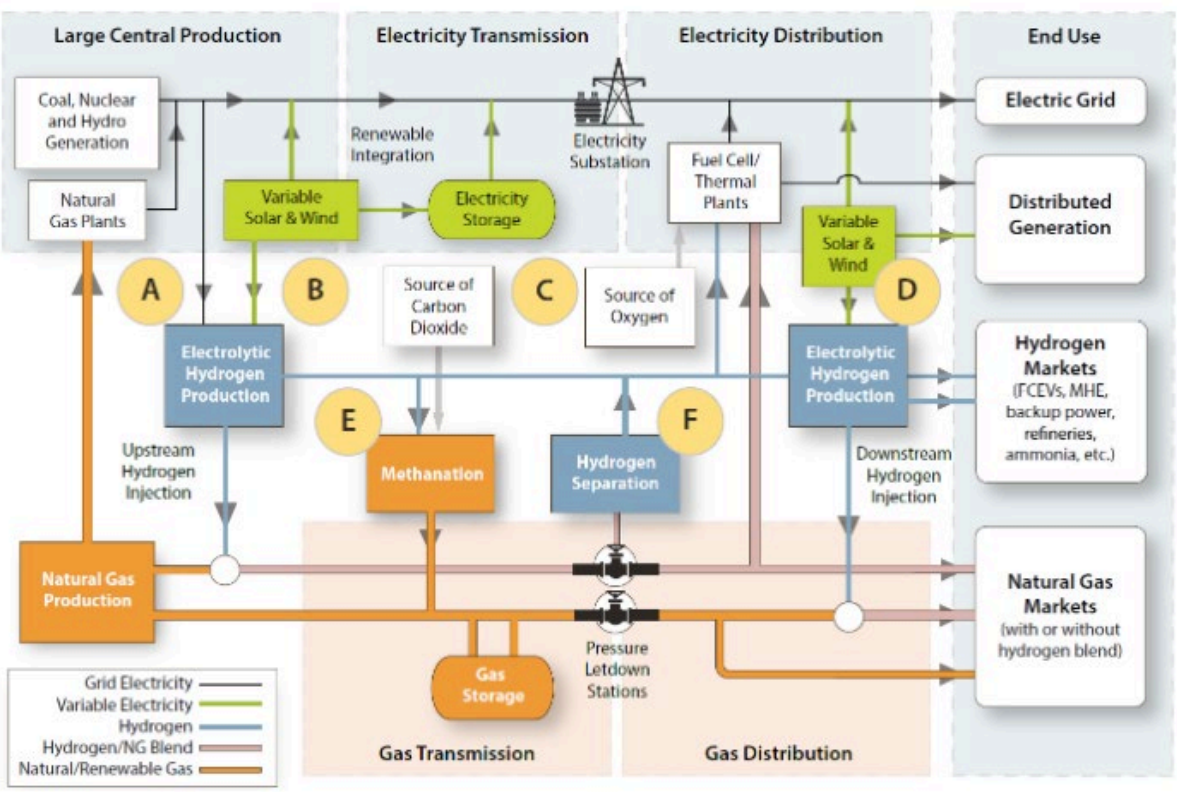

Figure 1. Pathways of hydrogen from production to storage and end-uses.
Source: [8].

Hydrogen is produced in various ways. Some well-known methods are water electrolysis, steam reforming, and thermochemical or biochemical processes. Of these methods, thermochemical and biochemical processes will require feedstock of methane and biomass to be supplied, which ultimately negates the intention to produce hydrogen to eliminate SLOC vulnerabilities. [12] The electrolysis of water and thermochemical production methods are described below.

A. WATER ELECTROLYSIS

The principles of water electrolysis are relatively straightforward, although very energy-intensive [13]. Water in liquid or vapor form can be split into hydrogen and oxygen by the complete reaction

$$2H_2O(l,g) \rightarrow 2H_2(g) + O_2(g) \qquad (2\text{-}1)$$

When no work is input, the temperature that this decomposition occurs at (T_d) is 4310°K. This temperature is not practical to achieve by conventional means. However, the input of work can help this reaction occur at much lower temperatures. Electrical work is one means of achieving this. The electrical energy required to induce these reactions is found by calculating the Gibbs free energy

$$\Delta H = \Delta G + T\Delta S \qquad (2\text{-}2)$$

where ΔH is the change in enthalpy and is equal to the total energy needed for the reactions to occur. ΔG is the Gibbs free energy and is equal to the amount of electrical energy required for the reaction. T is the fluid temperature, and ΔS is the change in entropy. The ΔH required to split water from a condensed state to gaseous constituents is commonly called the Higher Heating Value (HHV), while the ΔH starting from a gaseous state to gaseous constituents is called the Lower Heating Value (LHV) [14].

The ΔH and ΔS required for these reactions are relatively constant [15], which means from eq. 2–2, if the water temperature goes up, the required amount of electrical energy will go down. This effect is shown in Figure 2, where the electrical energy needed

for the reactions has a downward trend as the water temperature goes up. The discontinuity in the data at 100°C is a result of the water vaporization and entopic change before and after vaporization.

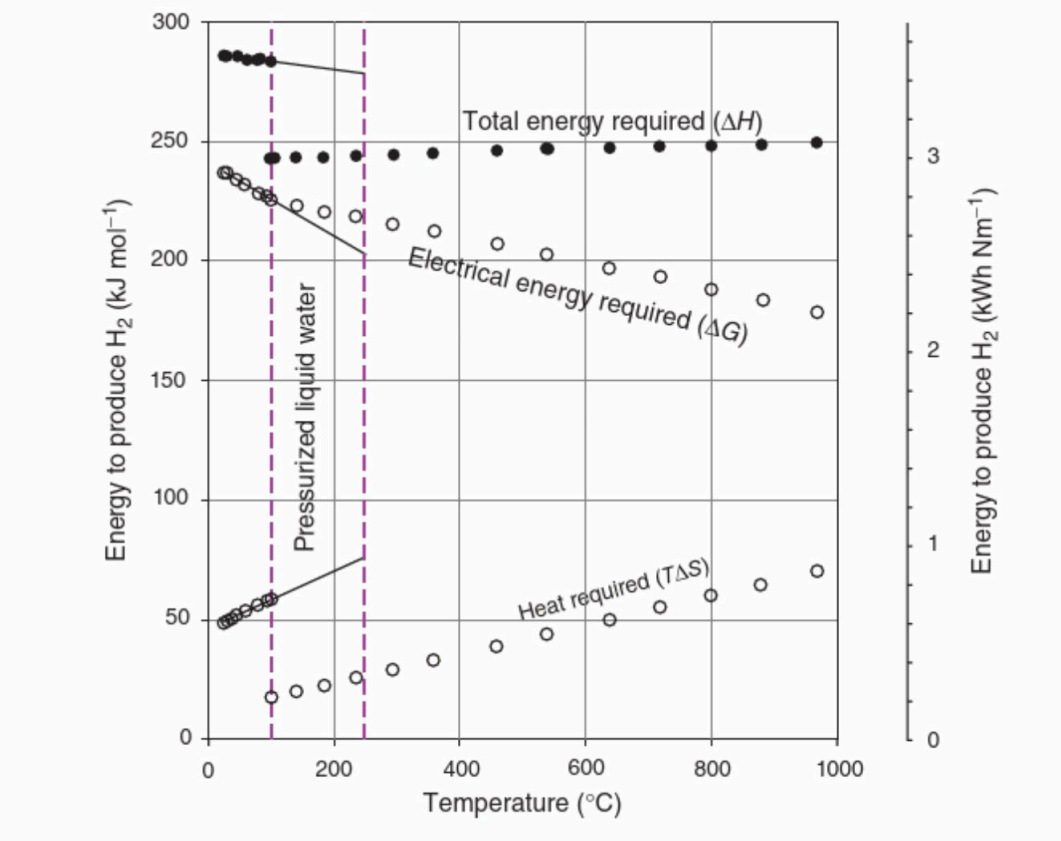

Figure 2. ΔG(T), ΔH(T), TΔS(T) of the water-splitting reaction at P = 1 bar (—) for pressurized liquid water up to 250°C. Source: [15].

1. Alkaline Electrolysis

The oldest method for creating hydrogen from water is through alkaline electrolysis. It is also one of the easiest methods due to its simple design and cheap materials. Alkaline water electrolysis (AWE) uses a diaphragm to separate the anode and cathode of the electrolyzer that is submerged in an alkaline solution (typically KOH). The anions from the strong base act to transfer the electricity between the electrodes, and the diaphragm is permeable by hydroxyls (OH^-) but not permeable to hydrogen and oxygen in

steady-state conditions. In this way, when a voltage is applied across the electrodes, the following reactions occur:

$$Anode:\ 4\,OH^- \rightarrow\ O_2 + 2\,H_2O + 4\,e^- \tag{2-3}$$

$$Cathode:\ \ 4\,H_2O +\ 4\,e^- \rightarrow 2\,H_2 + 4\,OH^- \tag{2-4}$$

The cells used for AWE are typically one of two designs. The first design is the unipolar cell, shown in Figure 3. The cell's electrodes, separated by a diaphragm, are submerged in a tank with an electrolytic solution in a parallel arrangement. The produced gases will exit out of the top of the cell. These cells are simple to produce and reliable, but the current density is less than other designs. The second AWE cell type is a bipolar cell, shown in Figure 4. Bipolar cells are connected serially and require the electrolyte solution to be circulated through the cell with pumps. The formed gasses circulate with the solution and are collected in reservoirs away from the cell. Bipolar cells are more compact and efficient than unipolar but are also more complex and require constant circulation. Most AWE systems operate in the temperature range of 60–80°C with an efficiency of 65–75% [15], [16]. Table 1 provides reference parameters for state-of-the-art specifications for the AWE electrolysis cells.

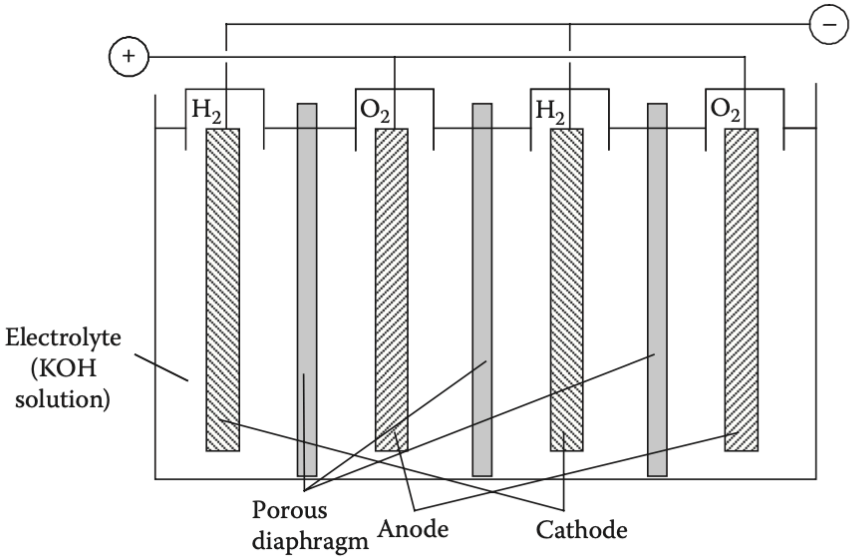

Figure 3. Schematic of a unipolar AWE cell. Source: [17].

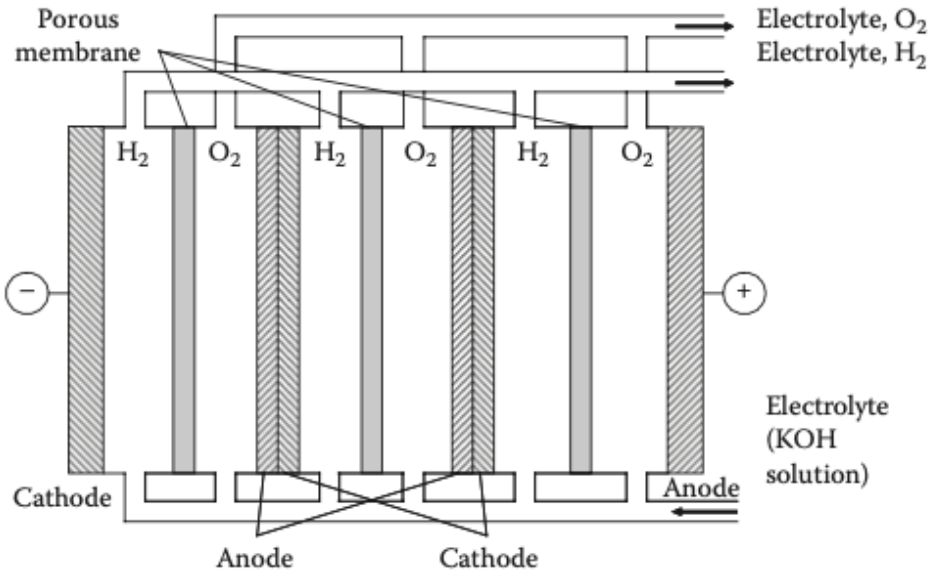

Figure 4. Schematic of a bipolar AWE cell. Source: [17].

Table 1. State-of-the-art alkaline electrolysis specifications. Adapted from [18].

Cell Temperature (°C)	60 -80
Cell pressure (bar)	<30
Current Density (mA cm^{-2})	0.2 – 0.4
Cell voltage (V)	1.8 – 2.4
Power density (mW cm^{-2})	<1
Voltage efficiency HHV (%)	62 – 82
Specif. energy consumption: Stack (kW h Nm^{-3})	4.5 – 7.0
Specif. energy consumption: System (kW h Nm^{-3})	4.5 – 7.0
Lower partial load range (%)	20-40
Cell area (m^2)	>4
H_2 production rate: Stack-system (Nm^3 h^{-1})	<760
Lifetime stack (h)	<90,000
Lifetime system (y)	20-30
Degradation rate (μV h^{-1})	<3

AWE has several advantages over other water electrolysis methods that make it a competitive option for use with an LFR [15], [16], [18].

- Simple in design and can be made with inexpensive materials. Commercial systems already exist with power in the MW range.
- Very high purity of gas products
- Because AWE has the most extended history of any hydrogen production method, there is abundant experience and research from which to build.

Disadvantages of AWE include [15], [16]:

- AWE is limited in operating temperature to <100°C due to the electrolytic solution's corrosive nature and chemical instability at high temperatures.
- At high current densities, AWE experience an increase in ohmic resistance due to gaseous bubbles suspended in solution. Operations at higher

pressure can mitigate this, but that introduces complexities and safety issues to the system's design.

- AWE must be run at a constant level because transients in operation will cause an imbalance to partial pressure values that will force the diffusion of product gasses across the membrane

2. PEM Electrolysis

One of the most well-established methods of water electrolysis is the use of Polymer Electrolyte Membrane (PEM) cells. Initially, they were developed for oxygen production in anaerobic environments like space crafts or submarines. PEM cells use a proton-conduction polymer electrolyte to separate the anode and cathode. The water is separated at the anode by

$$H_2O(l) \rightarrow \frac{1}{2}O_2(g) + 2H^+ + 2\,e^- \tag{2-5}$$

Where the oxygen formed at the anode can be collected at the top of the cell. The H^+migrates through the membrane to the cathode and forms hydrogen gas by

$$2\,H^+ + 2\,e^- \rightarrow H_2(g) \tag{2-6}$$

Figure 5 shows a diagram of a typical cell configuration and flow of the PEM process. Additional water is shown flowing across the polymer membrane by electro-osmosis drag. PEM electrolyzers typically operate between 50 and 80°C due to the limitations of the Polymer membrane. Reference specifications for state-of-the-art PEM electrolyzers are summarized in Table 2.

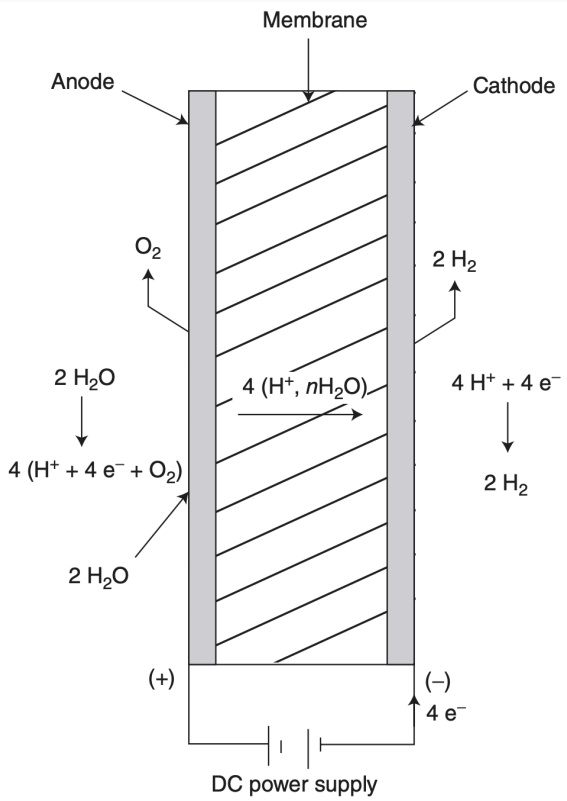

Figure 5. PEM cell diagram. Source: [16].

Table 2. State-of-the-art PEM specifications. Adapted from [18].

Cell Temperature (°C)	50 -80
Cell pressure (bar)	<30
Current Density (mA cm^{-2})	0.6 – 2.0
Cell voltage (V)	1.8 – 2.2
Power density (mW cm^{-2})	<4.4
Voltage efficiency HHV (%)	67 – 82
Specif. energy consumption: Stack (kW h Nm^{-3})	4.5 – 5.6
Specif. energy consumption: System (kW h Nm^{-3})	4.5 – 7.5
Lower partial load range (%)	0-10
Cell area (m^2)	<0.03
H_2 production rate: Stack-system (Nm^3 h^{-1})	<10
Lifetime stack (h)	<20,000
Lifetime system (y)	10-20
Degradation rate (μV h^{-1})	<14

PEM electrolysis has several advantages over other methods [19], [16].

- PEM does not require a liquid electrolyte, so more options exist for cheap structural materials.
- The faradic efficiency is better because there are no gas bubbles between electrodes that would cause ohmic losses. This allows for higher current density.
- The hydrogen gas purity is very high, with no solution droplets suspended in the gas.
- The separation of the electrodes can be minimal and contribute to a compact system design.
- PEM cells can withstand significant pressure differences and are not as susceptible to transient conditions as AWE.

Disadvantages of the PEM method include the following [16], [15].

- The most significant disadvantage of PEM electrolysis is the high cost of the required electrodes that need to be corrosion resistant against the acidic polymer material.
- The operating temperature is limited by the stability of the polymer material used. This limits the achievable efficiency of the system.
- Fabrication of cells is difficult to meet uniform contact requirements to reduce electrical resistance.

B. STEAM ELECTROLYSIS/SOLID OXIDE ELECTROLYSIS

One way to reduce the amount of electricity required to stimulate the water-splitting reaction is to use high-temperature steam in a solid-oxide electrolyzer cell (SOEC). This process is known as High-Temperature Steam Electrolysis (HTSE) and is well documented

in the research literature [15], [16], [20], [21]. A diagram of a typical SOEC cell is shown in Figure 6. Steam flowing into a SOEC will be disassociated at the cathode by

$$H_2O + 2\,e^- \rightarrow\ H_2 + \frac{1}{2}O^{2-} \tag{2-7}$$

The negatively charged oxygen is transported to the anode through a gas-tight, oxygen-ion conducting electrolyte, while the highly purified H_2 can be separated from the residual steam by condensation. The oxygen collects at the anode, where it releases its electrons through the following reaction:

$$2\,O^- + 2\,e^- \rightarrow\ O_2 \tag{2-8}$$

The gaseous oxygen is then collected on the anode side of the cell. The operating temperature for HTSE is typically between 800–1000°C [17] which would be too high for heat transfer directly from the reactor coolant. This high cell temperature is required due to adverse electrical properties of the oxygen-ion-conducing electrolyte material at low temperatures. However, research with a proton-conducting electrolyte has successfully lowered the operating temperature to <600° [20], which would be compatible with an LFR. The reference characteristics of a SOEC are listed in Table 3.

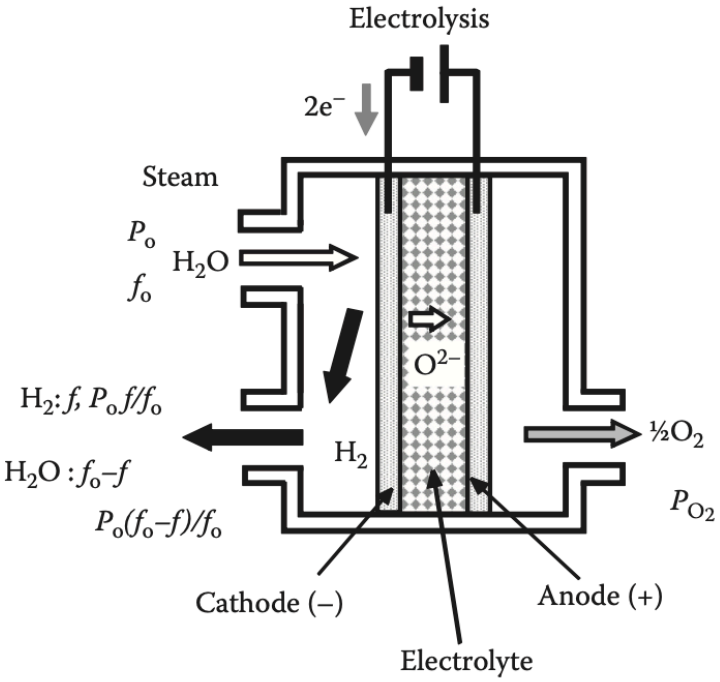

Figure 6. Illustration of high-temperature electrolysis of steam. Adapted from [15].

Table 3. SOEC operating characteristics. Adapted from [20], [21].

Cell Temperature (°C)	500-600
Cell pressure (bar)	<30
Current Density (mA cm^{-2})	.5 – 2.5
Cell voltage (V)	1 – 1.8
Voltage efficiency HHV (%)	67 – 82
Steam Utilization (%)	~80

The main benefit of steam electrolysis is reducing the electrical energy required for hydrogen production shown in Figure 2. Though the total energy (ΔH) required for splitting is relatively constant across a wide temperature range, the heat input (TΔS) from raising the temperature of the steam has lowered the required electrical input (ΔG) [22].

Some advantages of HTSE are summarized below:

- The high operating temperatures of HTSE significantly reduce the energy required to produce product gases.
- SOEC materials are relatively inexpensive and easy to produce [20].

Disadvantages of HTSE include:

- Most SOECs operate at very high temperatures (800-1000°C) that are not achievable by an LFR. Using a proton-conducting electrolyte in the SOEC could potentially lower this temperature to <600°, but more research is required for these materials [20].
- SOECs experience degradation and sealing issues due to their extreme operating environments [20].
- HTSE is a relatively new technology, and few operational systems have been developed. However, SOEC technology is similar to Solid Oxide Fuel Cells (SOFC), which have received an abundance of attention and funding for further research as the demand for clean energy sources has increased [16].

C. THERMOCHEMICAL/HYBRID PROCESSES

A significant advantage shown with the SOE method of hydrogen production is the reduced electrical input required to decompose a water molecule due to the high heat input. Another means of lowering this required electrical contribution is through chemical reactions. One of the most popular thermochemical production methods is the iodine-sulfur (IS) process [17], [23]. A pure thermochemical reaction (without any external inputs) consists of three reactions. In the first reaction, eq. 2–9, iodine reacts with Sulfur dioxide and water at low temperatures to create products hydrogen iodide and sulfuric acid. When heated at different temperatures in a process, these products decompose by the reactions shown in eq. 2–10 and eq. 2–11 to create the desired hydrogen and oxygen products.

$$I_2 + SO_2 + 2H_2O \rightarrow 2HI + H_2SO_4 \ (20\text{-}100\ C) \tag{2-9}$$

$$2HI \rightarrow H_2 + I_2 \ (200\text{-}700\ C) \tag{2-10}$$

$$H_2SO_4 \rightarrow SO_2 + H_2O + \frac{1}{2}O_2 \ (850\ C) \tag{2-11}$$

Figure 7 also shows a diagram demonstrating the overall process and temperature requirements for the different reactions. It is noted in these reactions that significant heat input is necessary to achieve the required temperature for eq. 2–12 to occur [24], [25].

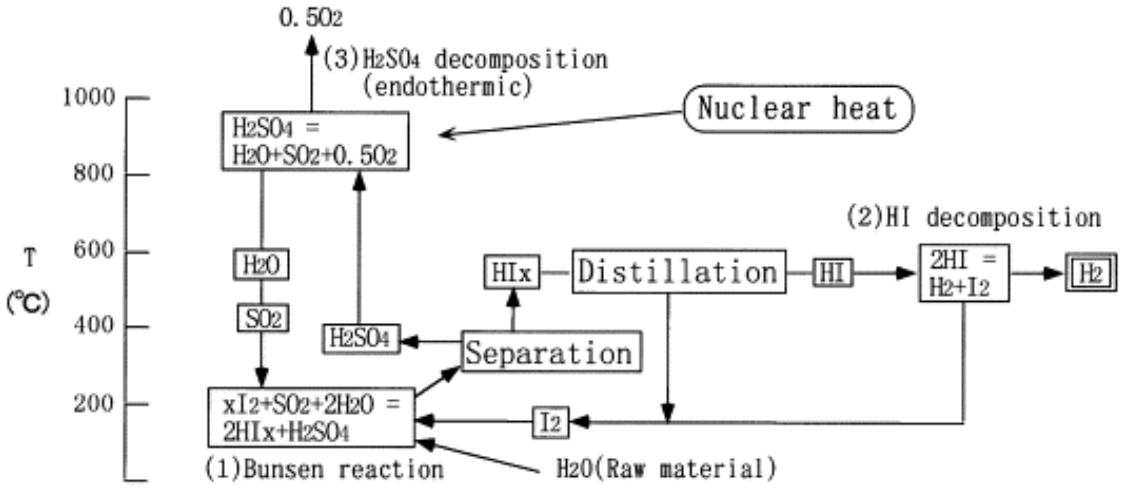

Figure 7. IS process (no electrical input). Source: [25].

One means of overcoming the temperature barrier for a thermochemical reaction is to utilize electricity in a hybrid process. There have been many studies on hybrid methods attempting to make hydrogen production by this means feasible and sustainable. One promising study conducted by the Japan Atomic Energy Agency (JAEA) uses electrolysis to lower the temperature required to approximately 500C [26]. This method uses sulfuric acid water-cracking to produce hydrogen by

$$SO_3 \rightarrow SO_2 + \frac{1}{2}O_2 \tag{2-12}$$

$$2H_2O + SO_2 \rightarrow H_2SO_4 + H_2 \quad (2\text{-}13)$$

$$H_2SO_4 \rightarrow H_2O + SO_3 \quad (2\text{-}14)$$

Where electrolysis is used in the processes of eq. 2–12 to lower the required temperature of the endothermic reactions to one attainable by an LFR. Electrolysis is used in eq. 2–13 with cooling at 50°C because this is an exothermic reaction. Altogether, the hybrid sulfur water-cracking method can reduce the electricity requirements for hydrogen production by as much as two-thirds compared to conventional water electrolysis [17]. Figure 8 shows a diagram of the different phases of the proposed hybrid process with approximate temperatures for each reaction.

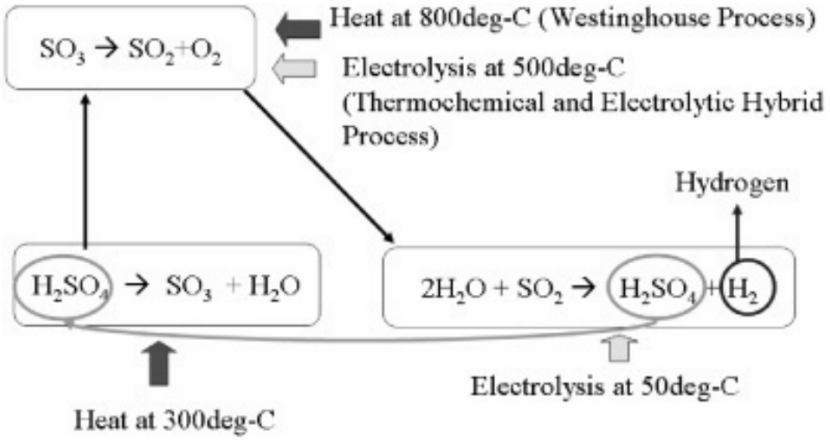

Figure 8. Diagram of hybrid thermochemical electrolysis process with approximate phase temperatures. Source: [26].

Advantages of the Thermochemical production process include:

- Thermochemical cycles require less electrical input to force water-splitting reactions [27].
- Compared to HTSE, Thermochemical processes can be operated at lower temperatures.

- Engineering challenges and losses due to membranes are avoided since gases are separated without the need for membranes. This is not the case for hybrid reactions, which still need separation for the electrodes.

Some disadvantages of a Thermochemical cycle are:

- Chemical engineering challenges such as undesirable by-products, unreacted reactants, and separation of reaction products are a significant disadvantage to Thermochemical cycles [17].
- The time required for reactions to occur forces recirculation of reactants and creates thermal inefficiencies [17].
- Materials required to sustain the high temperatures and corrosive environment drive up the cost of production for Thermochemical cells [17].
- For hybrid cycles, by-products can deposit on the electrodes and impact the cycle's efficiency

THIS PAGE INTENTIONALLY LEFT BLANK

III. LEAD COOLED FAST REACTORS

Lead Cooled Fast Reactors (LFR) are not new. Most notably, the Soviets used LFRs to power their Alfa Class of submarines. Fifteen cores in total were produced and contributed to decades of research on LFR operations and design. Compared to their American competitors' light-water reactors (LWR), these were more fuel and energy-efficient, smaller, and operated at a safer pressure [28]. The Generation IV International Forum (GIF) identified LFRs as one of the most promising technologies to meet the energy needs of remote locations due to their robust and passive safety characteristics. These advantages make LFRs ideal for use in hydrogen production in an EABO environment [29]. A small modular reactor (SMR) like the Small Secure Transportable Autonomous Reactor (SSTAR) conceptualized and designed by a team led by Lawrence Livermore National Laboratory would be particularly well suited for this application and is the reference system for this analysis.

A. BREEDER REACTOR BASICS

An LFR is a uranium or mixed uranium-plutonium fueled, fast neutron spectrum, breeder reactor that generates fissile material to use as fuel as it operates. Unlike pressurized water reactors, which moderate the neutron flux to a thermal level, the heavy nuclei in LFRs have a small moderation effect and act as good neutron reflectors to prevent fast neutrons from escaping from the core. These properties make LFRs ideal as a breeder reactor. Breeder reactors use high neutron flux and a fertile fuel component, like uranium-238, to create more fissile material than they consume. Figure 9 illustrates the breeding process from a neutron interaction with fertile Uranium-238 to the fissionable Plutonium-239. Because of this breeding process that creates fissionable fuel, LFRs have very high fuel efficiency and can operate for 15–30 years without refueling.

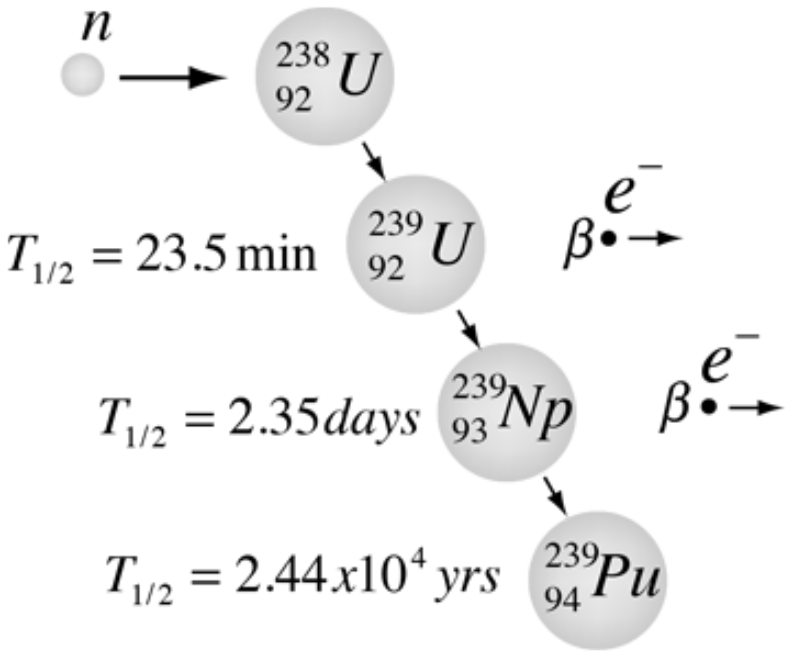

Figure 9. Illustration of the breeding production of fissionable Plutonium-239 from fertile Uranium-238. Source: [30].

B. LEAD AS A COOLANT

LFRs commonly use a pure lead or lead eutectic mixture with bismuth (LBE) for a coolant. Lead provides several advantages over other alternatives.

- As a heavy metal, lead acts to scatter high-energy neutrons through elastic collisions and has a low cross-section of absorption that maintains a high fast neutron spectrum needed for breeding [31].
- Lead and LBE have high boiling points and low saturation pressures, making these metals better from a safety standpoint because the plant can be operated at ambient pressures. The risk of a void forming in the core from coolant boiling is virtually eliminated [32].
- Chemically, Lead and LBE are effectively chemically inert. Unlike Sodium-cooled reactors, they have little reaction to water or air [32].
- Lead and LBE provide inert shielding from gamma radiation [32].

- Because of their thermodynamic properties, Lead and LBE can be used to cool the reactor passively through natural circulation [33].

Some disadvantages of using Lead and LBE include:

- Both Lead and LBE exhibit high corrosive attacks on conventional structural material at high temperatures. This limits the operating temperature of LFRs until more research and development (R&D) can be conducted to determine compatible corrosion-resistant alternatives and chemical environments that can limit corrosive attack [32].

- The melting temperatures for Lead (327°C) and LBE (125°C) are high enough to pose engineering and operational challenges to ensure the coolant does not freeze and cause flow blockage [32].

- LBE and, to a lesser extent, pure Lead can create hazardous, radioactive products from activation. The primary concern is Polonium-210 which is radiotoxic, volatile, and significantly contributes to heat generation in the core, especially after shutdown. Polonium-210 is primarily a concern when using LBE as a coolant for the subsequent activation.

  $^{209}Bi + n \rightarrow {}^{210}Bi$ (β- ; $t_{1/2}$ 5 days) $\rightarrow {}^{210}Po$ (α ; $t_{1/2}$ 138.4 days)

C. SUPERCRITICAL CO_2 BRAYTON CYCLE

Unlike LWRs that are typically coupled with a Rankine thermodynamic cycle and use steam as a working fluid, S-CO_2 Brayton cycles use Carbon Dioxide in a supercritical state as a working fluid. A supercritical fluid is a fluid state above its critical temperature and pressure that makes the fluid adopt both gas and liquid properties. Typically, supercritical fluids are dense like a liquid but compressible like a gas. The amount that the fluid acts like either a gas or a liquid state can be tuned by changes in operating pressure or temperature. This provides several advantages over conventional Rankine cycles [34], [35].

- S-CO_2 density is much greater than other working fluids, allowing for a higher power density and significantly smaller turbines and compressors.
- There is potential for higher plant efficiency and optimization with no fluid phase transitions.
- Reduced water consumption and dry cooling capability suitable for arid environments

Figure 10 illustrates a basic S-CO_2 Brayton cycle, and Figure 11 shows a corresponding Total Entropy (S) vs. Temperature (T) diagram. At the first point in the cycle, heat exchangers in the reactor heat the supercritical fluid to high temperatures (1). The fluid then performs work on the turbine driven by the pressure difference across the turbine (2), causing it to rotate and produce electrical power with the generator. Next, excess heat is rejected by the system when the fluid is cooled to near the critical temperature by the recuperator (3) and cooler (4). A compressor (5) then increases the fluid pressure before reheating it to the required inlet temperature for the reactor by the recuperator (6). Finally, the high-pressure fluid re-enters the reactor to repeat the cycle (1) [36].

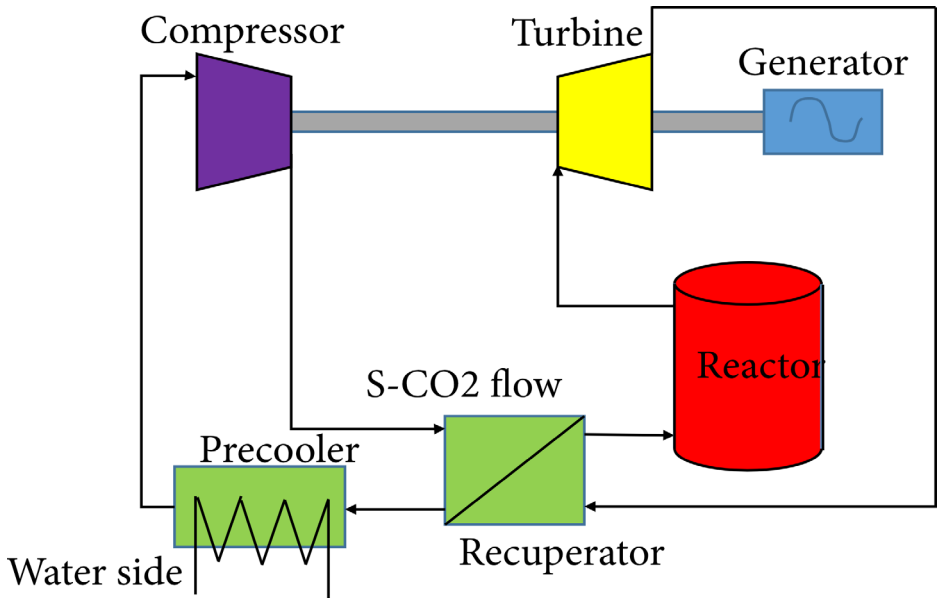

Figure 10. Schematic of a S-CO_2 Brayton cycle coupled to a reactor. Source: [36].

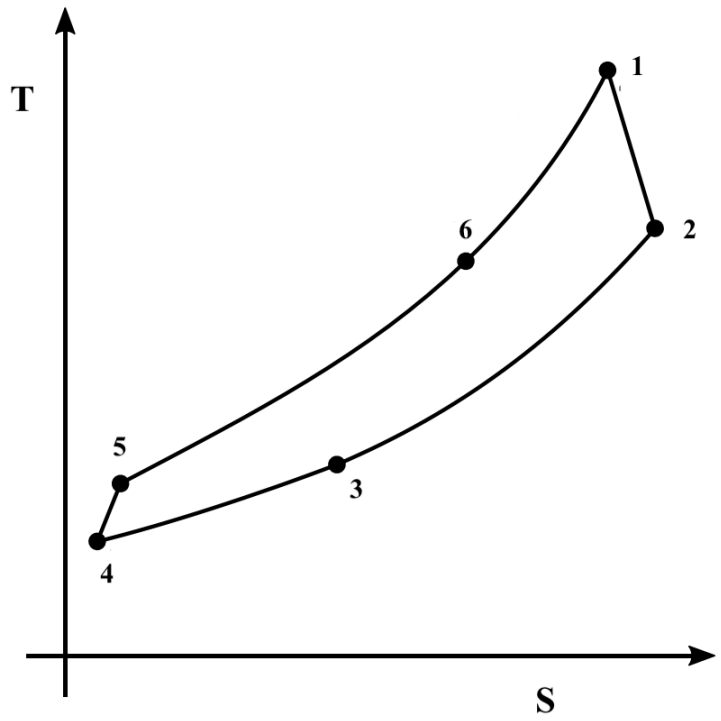

Figure 11. Absolute entropy (S) vs. temperature for an S-CO_2 Brayton Cycle. Adapted from [37].

Though the S-CO_2 Brayton cycle has many advantages over other energy conversion cycles, it also has several drawbacks that introduce design challenges. [37]

- The dynamic nature of the fluid properties (like specific heat) near the critical point makes the system very sensitive to changes in temperature and pressure. This will require appropriate system regulation to maintain optimal conditions.
- The critical point of CO_2 limits the system to a minimum pressure of 73.9 bar, which lowers the attainable pressure ratio. This ultimately limits the achievable efficiency of the system.
- CO_2 is highly corrosive at the required temperatures for the system operations. This requires further development and testing of materials used in these conditions.

D. SMALL SECURE TRANSPORTABLE AUTONOMOUS REACTOR (SSTAR)

In the early 2000s, Lawrence Livermore National Laboratory organized a collaborative effort across multiple universities and national laboratories to develop the Small Secure Transportable Autonomous Reactor. The intended purpose of this effort was to create an SMR that could be safe and transportable enough to operate in remote environments for extended periods and require minimal manning and upkeep. Figure 12 shows a basic schematic of the SSTAR core design, and Figure 13 illustrates the plant's integration with the S-CO_2 Brayton cycle and calculated conditions. Table 4 provides technical design parameters. The system would be sealed and designed to have a core life of approximately 30 years, so refueling would not be necessary. SSTAR uses a Lead cooled, transuranic Nitride fuel that provides strong temperature feedback of reactivity that allows for autonomous load following and minimizes control rod movement. The system allows natural circulation to meet all operational and shutdown cooling needs [38], [39], [40].

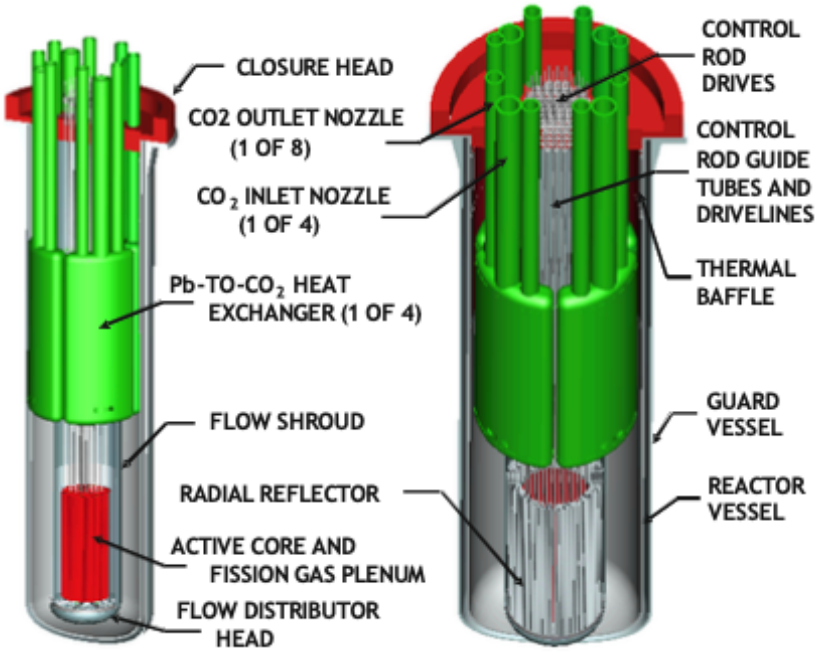

Figure 12. Schematic of the SSTAR LFR. Source [38].

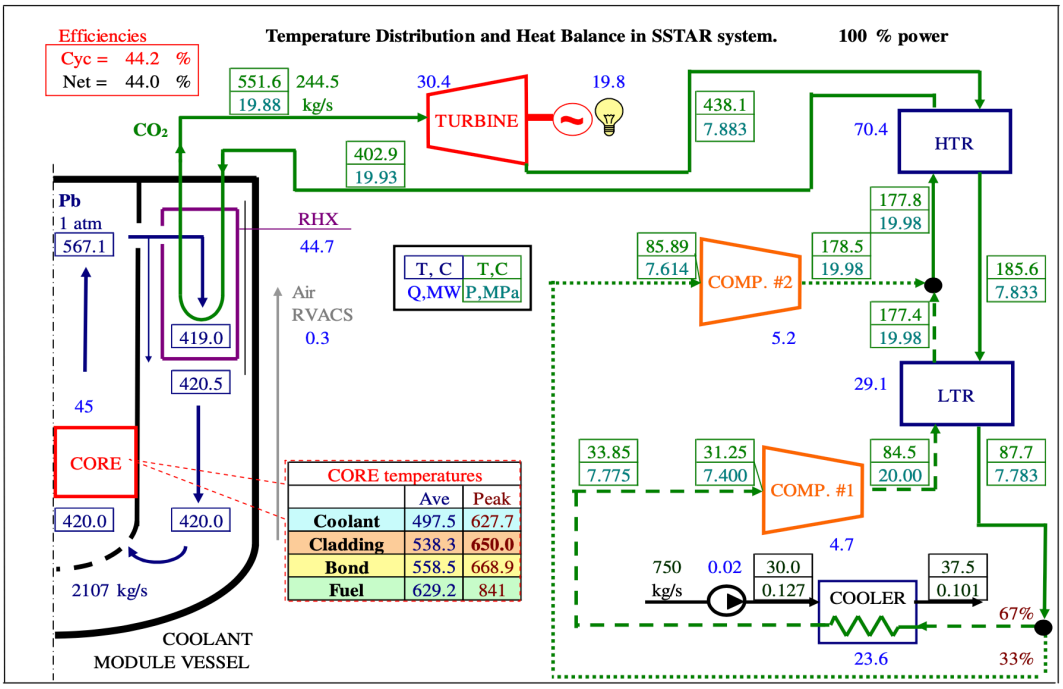

Figure 13. Schematic of SSTAR coupled with S-CO_2 Brayton cycle showing calculated conditions. Source: [39].

Table 4. SSTAR system parameters. Adapted from [39].

Coolant	Pb
Coolant Circulation	Natural Convection
Power Conversion	Supercritical CO_2, Brayton cycle
Fuel	TRU Nitride w/ enriched ^{15}N
Enrichment (%)	5 radial zones; 1.7/3.5/17.2/19.0/20.7
Core Lifetime, year	~30
Core inlet/outlet Temperature °C	420 / 567
Coolant Flow Rate, kg/s	2107
Power density, W/cm^3	42
Average (peak) discharge burnup, MWd/kg HM	81 (131)
Burnup Reactivity Swing, $	<1
Peak fuel temperature °C	841
Cladding	Silicon-enhanced ferritic/martensitic SS bonded to fuel pellets by Lead
Peak cladding temperature, °C	650
Fuel/coolant volume fractions	0.45 / 0.35
Core lifetime, years	15-30
Fuel pin diameter, cm	2.50
Fuel pin Triangular pitch-to-diameter ratio	1.185
Active core dimensions height/diameter, m	0.976 / 1.22
Core hydraulic diameter	1.371

Pb-to-CO_2 HXs Type	Shell-and-Tube
Number of Pb-to-CO_2 HXs	4
HX Tube Length, m	4.0
HX Tube Inner/Outer Diameters, cm	1.0 / 1.4
Number of Tubes (all HXs)	10,688
HX Tube Pitch-to-Diameter Ratio	1.222
HX Pb Hydraulic Diameter, cm	0.904
HX -Core Thermal Centers Separation Height, m	6.80
Reactor Vessel Dimensions Height/Diameter, m	12.0 / 3.23
Reactor Vessel Thickness, cm	5.08
Gap Between Reactor Vessel and Guard Vessel, cm	12.7
Gap Filling Material	Air
Guard Vessel Thickness, cm	5.08
Air Channel Thickness, cm	15
Air Ambient Temperature, C	36
Working Fluid	Supercritical CO_2
CO_2 Turbine Inlet Temperature, C	552
Minimum CO_2 Temperature in Cycle, C	31.25
Max/Min CO_2 Pressure in Cycle, C	20/7.4
CO_2 Flow Rate, Kg/s	245
Net Generator Output, Mwe	19.8
Supercritical CO_2 Brayton Cycle Efficiency, %	44.2
Net Plant Efficiency, %	44.0

IV. METHODOLOGY

Generally speaking, efficiency is measured as the ratio of the work produced by a system compared to the work put into a system. Typically for a reactor plant, this can easily be measured from the electrical energy generated and the energy produced by the reactor core. [41] In terms of hydrogen production, determining the efficiency of the overall process is not as straightforward and is dependent on the method and materials used and operating conditions. The amount of hydrogen produced by an electrolysis reaction is a function of the current density between the cell's electrodes

$$\dot{V_{H_2}} = \eta_F \frac{n_c I}{2F} V_{mol} \tag{4-0}$$

where $\dot{V_{H_2}}$ is the hydrogen production rate. η_F is the cell's faradaic efficiency (a measure of the current leakage). n_c is the number of cells connected in series. F is Faraday's constant, and V_{mol} is the molar volume for a gas at standard temperature and pressure (STP) [42].

The overall production rate of the system depends on several factors of cell design and operations. Parasitic reactions, leakage across boundaries and diaphragms, demands of auxiliary equipment, and any additional purification, drying, and condensing processes will affect the overall hydrogen production rate. [15] For the purposes of this thesis, each method needs to be evaluated individually to determine which process is best suited for pairing with an LFR in a remote operating environment. It will be assumed that design considerations to maximize production efficiency (such as material selection for electrodes and membranes, determining best cell operating pressures, or catalyst selection) are beyond the scope of this analysis. This assumption is made because they do not specifically pertain to how using an LFR affects hydrogen production.

A. OVERALL SYSTEM EFFICIENCY

One of the best measures of system performance is by an evaluation of the thermal efficiency (η_{sys}) found by [17]

$$\eta_{sys} = \frac{\Delta H_{HHV}}{\Sigma Q_{WS} + \Sigma W_{WS}} \tag{4-1}$$

where ΔH_{HHV} is the higher heating value (HHV) for the water-splitting reaction. ΣQ_{WS} is the sum of the heat input into the water-splitting reaction, ΣW_{WS} is the sum of the work input to the water-splitting reaction, and η_{WG} is the efficiency of a hydrogen fuel cell, assuming the hydrogen created will be used for electricity generation.

Figure 14 shows a total water splitting system diagram with a work/heat balance. The Energy Conversion cycle is assumed to be an S-CO_2 Brayton cycle but could be replaced with a more conventional Rankine cycle. This cycle supplies the required energy for water splitting and a heat pump. The Water Splitting portion can be any of the methods described in Chapter II at any temperature or pressure. In general, enthalpy and entropy balances can be made for the system that can be altered depending on the method of hydrogen production used.

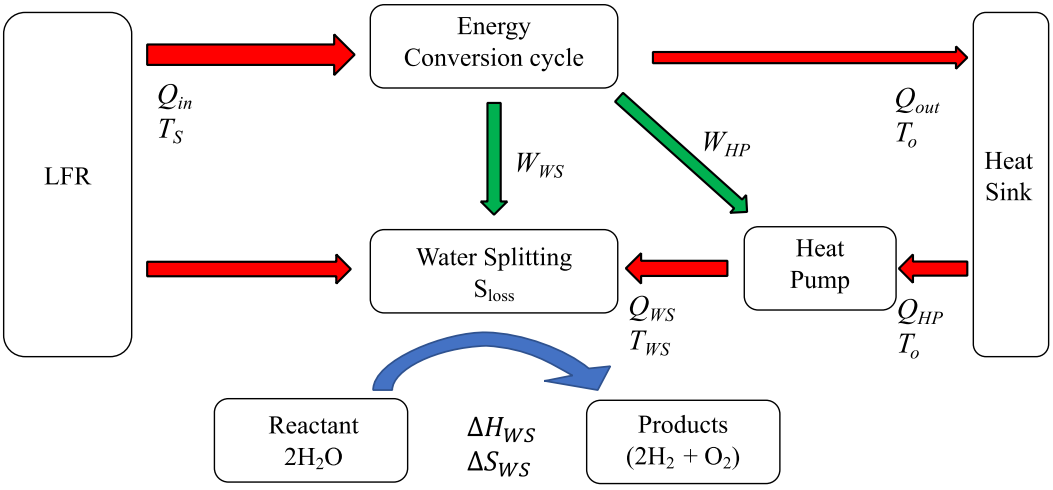

Figure 14. Heat and work balance for water splitting system. Adapted from [17].

B. S-CO_2 BRAYTON CYCLE EFFICIENCY

Chapter III describes how the reference LFR used for this analysis uses an S-CO_2 Brayton cycle for energy conversion, and there is a wealth of literature that describes methods for calculating the cycle efficiency [43], [44], [45]. The energy efficiency of the energy conversion cycle, η_{EC}, is found by

$$\eta_{EC} = \frac{\Sigma W + Q_{HL}}{Q_{in}} \tag{4-2}$$

Where ΣW is the net work from the coupled turbine and compressors shown by Eq. 4–2. Q_{HL} is the heat lost from the system described by Eqs. 4–3 and 4–4, and Q_{in} is the heat input into the system from the Reactor Heat Exchanger.

$$\Sigma W = \eta_t \left(\eta_m W_t - \frac{W_{comp}}{\eta_m}\right) \tag{4-3}$$

$$Q_{HL} = H_{cool,out} - H_{cool,in} \tag{4-4}$$

where η_t is turbine generator efficiency. η_m is the mechanism efficiency. W_t is the energy generated by the turbine from an isentropic expansion of the fluid and can be found from the change in enthalpy across the turbine through

$$W_t = H_{t,in} - H_{t,out} \tag{4-5}$$

W_{comp} is the Energy required for the compressors. $H_{cool,in}$ and $H_{cool,out}$ are the enthalpy values for the fluid coming into and out of the cooler, respectively. On examination of these equations, it is apparent that $H_{t,in}$, which is directly related to the LFR outlet temperature, will significantly impact cycle efficiency. In this way, as the reactor outlet temperature goes up, η_{EC} will go up as well. Figure 15 shows this relationship.

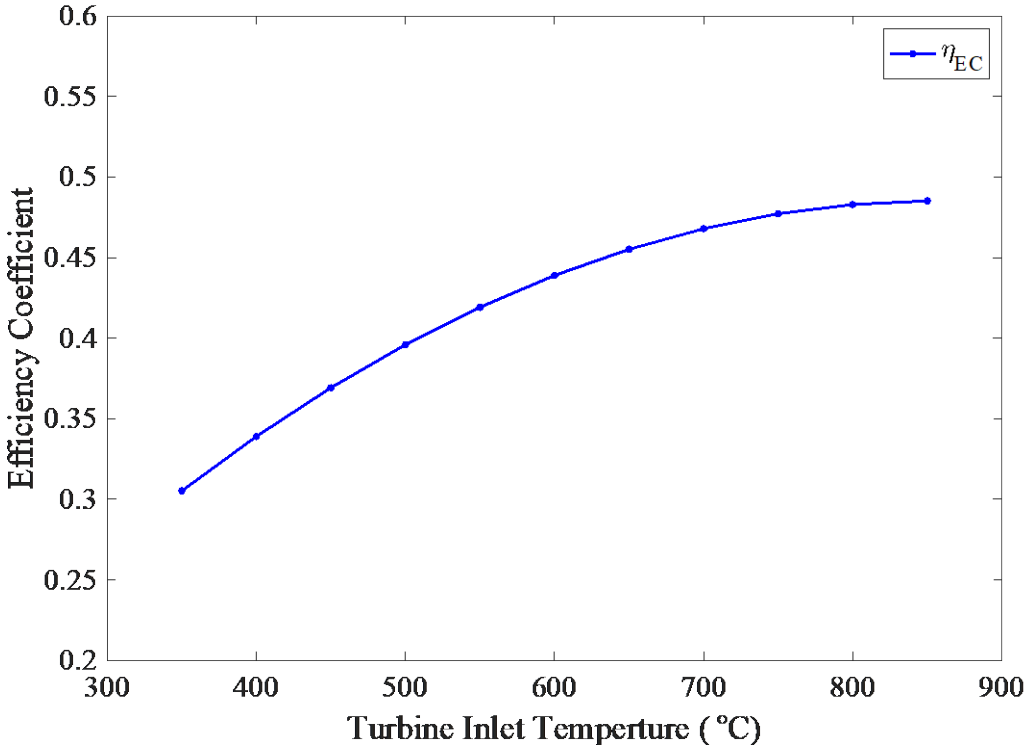

Figure 15. Efficiency of the S-CO_2 Brayton Cycle for SSTAR vs. inlet temperature. Adapted from [39].

C. ELECTROLYSIS EFFICIENCY

A cell's energy efficiency (η_e) can accurately measure an electrolyzer's performance independent of the subjective design characteristics described above. This method is well documented in the literature [15], [17], [14], [42], [46], [47] and is described in detail below.

The energy efficiency of an electrolysis cell is measured by comparing the HHV for the conditions of the fluid to the electricity and heat supplied to the system

$$\eta_e = \frac{HHV}{Electricty\ used + Heat\ supplied} \tag{4-6}$$

In other words, the energy efficiency is the ratio of work required for an ideal, reversible process (W_{rev}) to work required for a real, irreversible process (W_{irrev}).

$$\eta_e = \frac{W_{rev}}{W_{irrev}} \tag{4-7}$$

The reversible work can be found using the HHV value from thermodynamic tables as the enthalpy of formation, $\Delta_f H(T,p)$. This is expressed as

$$\Delta_f H(T,p) = \Delta_f G(T,p) + \Delta_f Q(T,p) \tag{4-8}$$

where $\Delta_f G(T,p)$ is Gibb's free energy of formation, analogous to the electrical energy requirement expressed by eq. 4–9, and $\Delta_f Q(T,p)$ is the thermal energy for formation found by eq. 4–10.

$$\Delta_f G(T,p) = z\,F\,V_{rev} \tag{4-9}$$

$$\Delta_f Q(T,p) = T\,\Delta_f S \tag{4-10}$$

where z is the number of electrons required to create a hydrogen molecule (z = 2). F is Faraday's constant (96485 C/mol). V_{rev} is the cell voltage for a reversible reaction. T is the cell's temperature, and $\Delta_f S$ is the change in entropy.

For work to be reversible, it must have 100% thermal efficiency (aka Thermoneutral) such that $\Delta_f S = 0$ and from Eq. 4–7, $\Delta_f H(T,p) = \Delta_f G(T,p)$. In this case, the Thermoneutral Voltage (V_{TN}) of the cell is expressed from Eq. 4–8 by

$$V_{TN} = \frac{\Delta_f H(T,p)}{z\,F} \tag{4-11}$$

And the reversible work is given by

$$W_{rev} = \Delta_f H(T,p) = z\,F\,V_{TN} \tag{4-12}$$

The real work required for electrolysis is simply the reversible work plus losses due to internal heating ($\Delta_{loss} Q$), as shown by

$$W_{irrev} = \Delta_f G + \Delta_f Q + \Delta_{loss} Q \tag{4-13}$$

$$\Delta_{loss} Q = n\, F\, \eta_{loss} \tag{4-14}$$

$$\eta_{loss} = V_{OCV} - V_{rev} \tag{4-15}$$

where $\eta_{loss}$is the irreversible voltage lost, and V_{OCV} is the open circuit cell voltage. V_{OCV} can be calculated from the Nernst equation as

$$V_{OCV} = V_{rev} - \frac{R\,T}{z\,F}\, ln\, (\frac{[H_2O]}{[H_2]\,[O_2]^{\frac{1}{2}}}) \tag{4-16}$$

Where *R* is the gas constant (8.314 J/mol K). *T* is the temperature in Kelvin, and "[…]" are the thermodynamic activity values approximated by associated partial pressure. Putting it all together, the energy efficiency (Eq. 4–6) can now be expressed by

$$\eta_e = \frac{W_{rev}}{W_{irrev}} = \frac{\Delta_f H}{\Delta_f H + \Delta_{loss} Q} = \frac{V_{TN}}{V_{TN} + V_{OCV} - V_{rev}} \tag{4-17}$$

Now that the effects of operational conditions on a cell's required voltage and efficiency are known, they can be compared back to how the overall production rate of hydrogen is affected given the reference conditions provided in Tables 1–3.

D. THERMOCHEMICAL/HYBRID EFFICIENCY

Thermochemical and hybrid water splitting reactions require less electrical energy than conventional electrolysis because they lower the heat requirement for a water-splitting reaction. Figure 16 shows this process. Reaction 3 is a typical water-splitting reaction. The required heat to force this reaction can be shifted to the left on the diagram by splitting the reaction into two steps (reactions 1&2). This can significantly lower the energy required to split water (HHV); however, Eq. 4–6 would still be applicable to measure the energy efficiency of these processes.

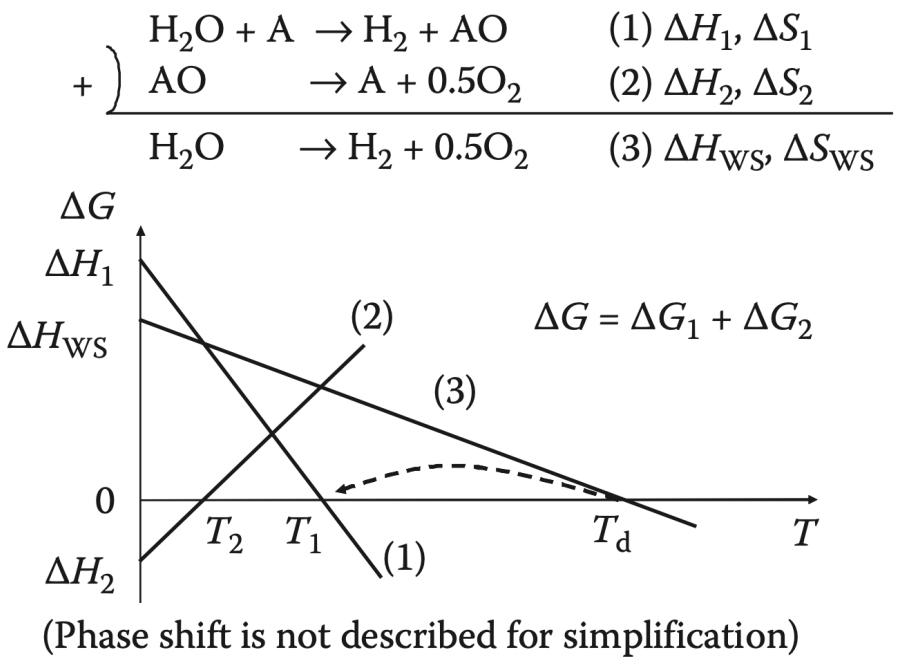

Figure 16. G-T diagram showing how a thermochemical alters $\Delta_f H$.
Source: [14].

THIS PAGE INTENTIONALLY LEFT BLANK

V. ANALYSIS RESULTS

The methods for finding system efficiency described in Chapter IV were used for each hydrogen production method paired with the reference SSTAR LFR. The results for each of these methods are described below.

A. PEM/ALKALINE WATER ELECTROLYSIS

Using the NIST-JANAF Thermochemical Tables (Appendix B) to find respective chemical formation values, the Thermoneutral voltage (V_{TN}) and Open-Circuit(V_{OCV}) was found as a function of temperature for a range of subcooled temperatures and plotted along with the cell's efficiency (η_e) in Figure 18. Of particular interest is the fact that the performance of the cells as measured by η_e goes down as temperature increases. This is likely because of the irreversible work performed in the form of internal heat generation at higher temperatures. As expected, V_{OCV} goes down as temperature increases which is beneficial for system designs because the amount of hydrogen produced is directly proportional to the current density in the cell. By Watt's law, then, less power is required for a given current

$$P_{elec} = V_{cell}\, I_{cell} \tag{5-1}$$

where P_{elec} is the electrical power required. V_{cell} is the operating cell voltage. I_{cell} is the current required for a given hydrogen production rate.

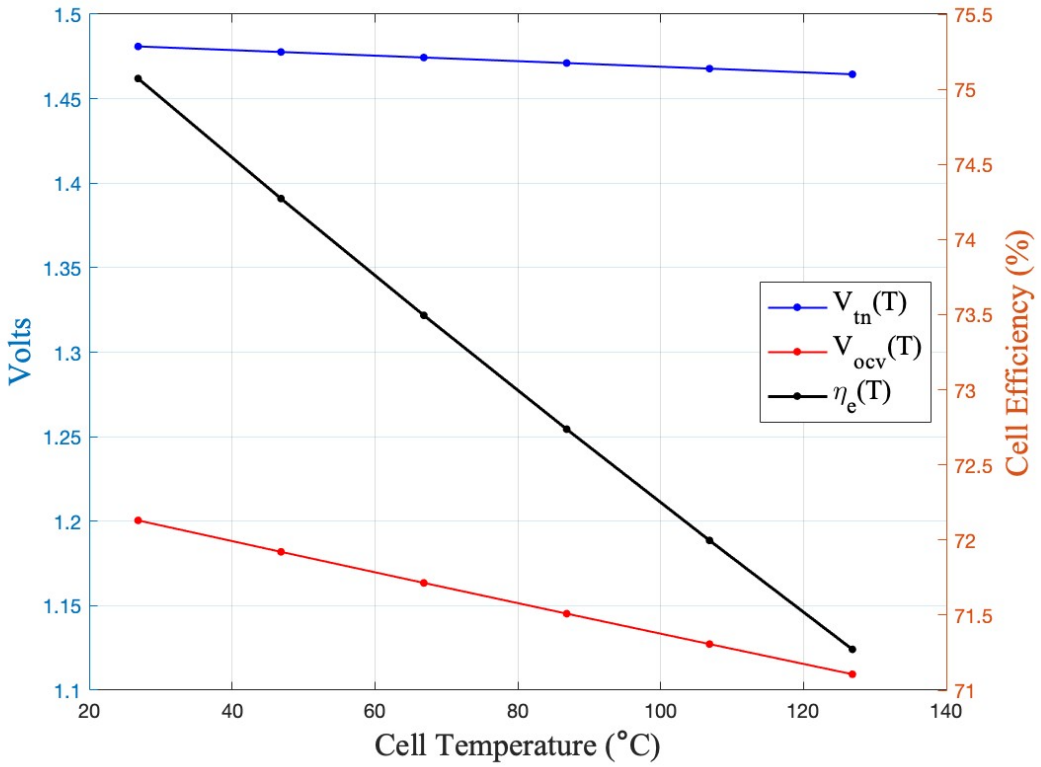

Figure 18. Thermoneutral voltage, open-circuit voltage, and cell efficiency vs. temperature for a PEM/AWE cell

Because of the similarity in operating characteristics for PEM and AWE, the two methods can be evaluated together as a single idealized case. In reality, differences in the polarization curves for the electrolytes used in the different methods will affect the actual cell performance. It was assumed for this analysis that the electrolyte material matched the characteristics of Nafion 115, which is commonly used in PEM cells [48]. Figure 19 is a polarization curve for this case based on the experimental results of [48] that shows how the cell's current (I_{cell}) changes as a function of cell voltage (V_{cell}) for different temperatures. At higher temperatures, there is less ohmic resistance; therefore, there is a higher I_{cell} for a given V_{cell} value at a higher temperature.

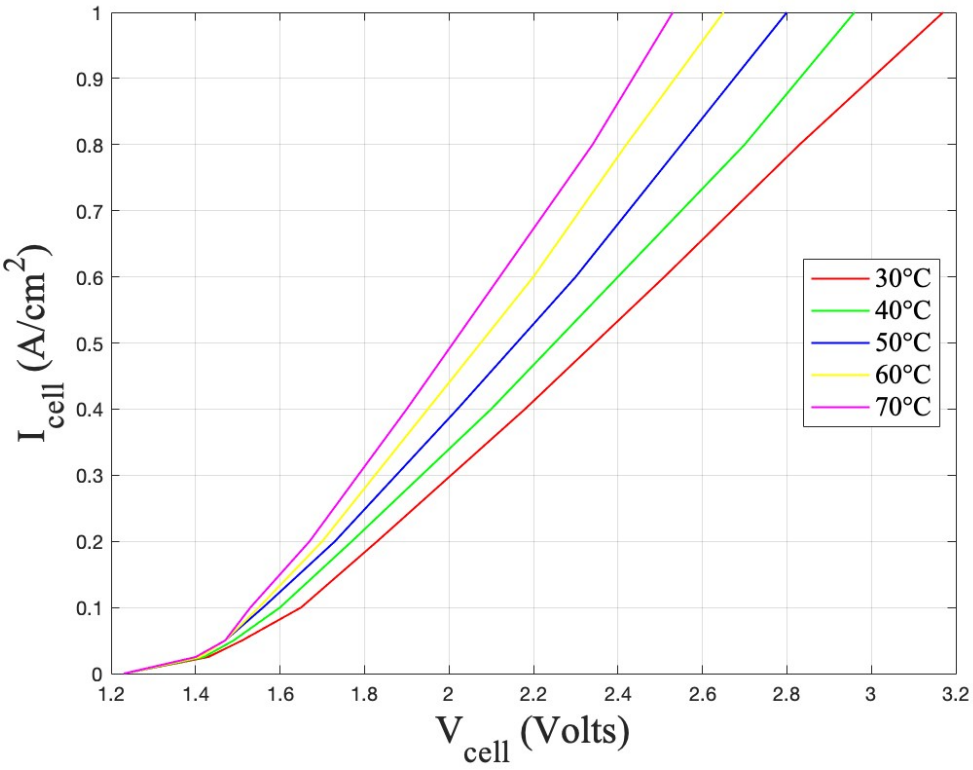

Figure 19. Polarization (aka I-V) plot for Nafion 115. Adapted from [48].

Using the polarization data from above, the power requirements for a single PEM cell were determined as a function of temperature, assuming a desired I_{cell} of 0.5 amps. This is shown in Figure 20. As expected, the power requirement for a given current goes down as the temperature increases. However, the change is not linear, and there is little benefit in increasing cell temperatures to more than 100°.

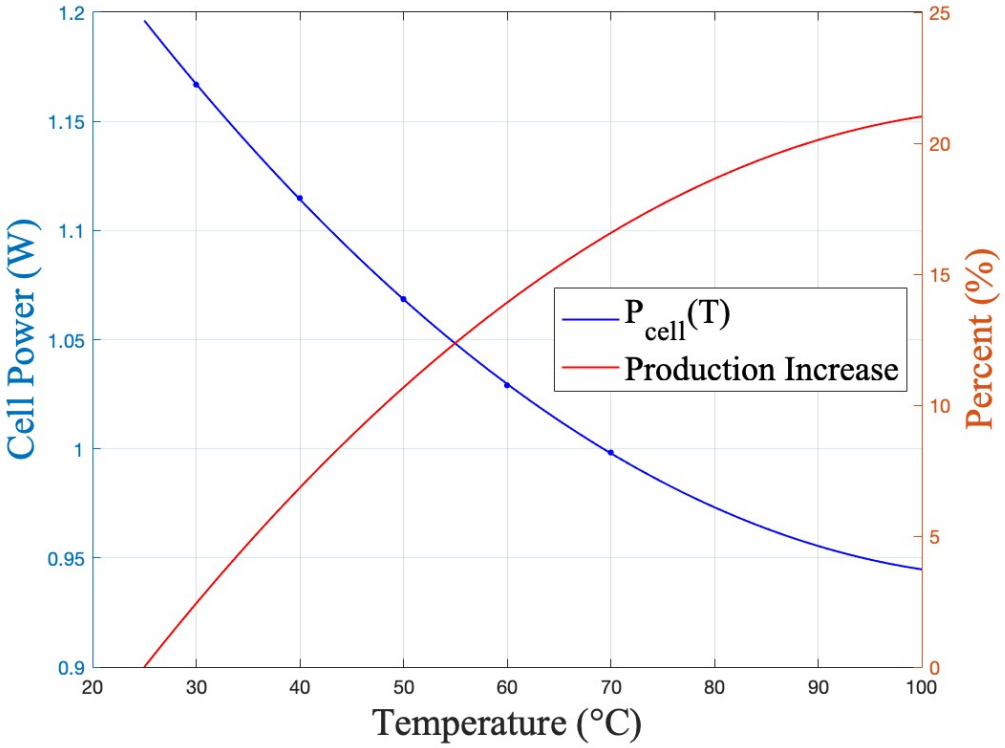

Figure 20. PEM cell power requirement as a function of temperature

The total reactor power required to achieve the cell voltages for hydrogen production is a combination of the power needed for electrolysis and the power needed to raise the temperature of the water in the system. At the lower temperatures of PEM electrolysis, it is assumed that a heat pump would be used to increase the solution water's temperature. This would limit the system's efficiency to the S-CO_2 cycle used or electricity generation (40%). Figure 21 shows the reactor power required for electrolysis (Cell Power) and power required to heat the water (Heating Power) from ambient to cell operating temperatures. Interestingly, the total reactor power required per cell (Total Power) goes up with operating temperature. This is due to inefficiencies of the system to heat the water using a heat pump or other electrical heating method.

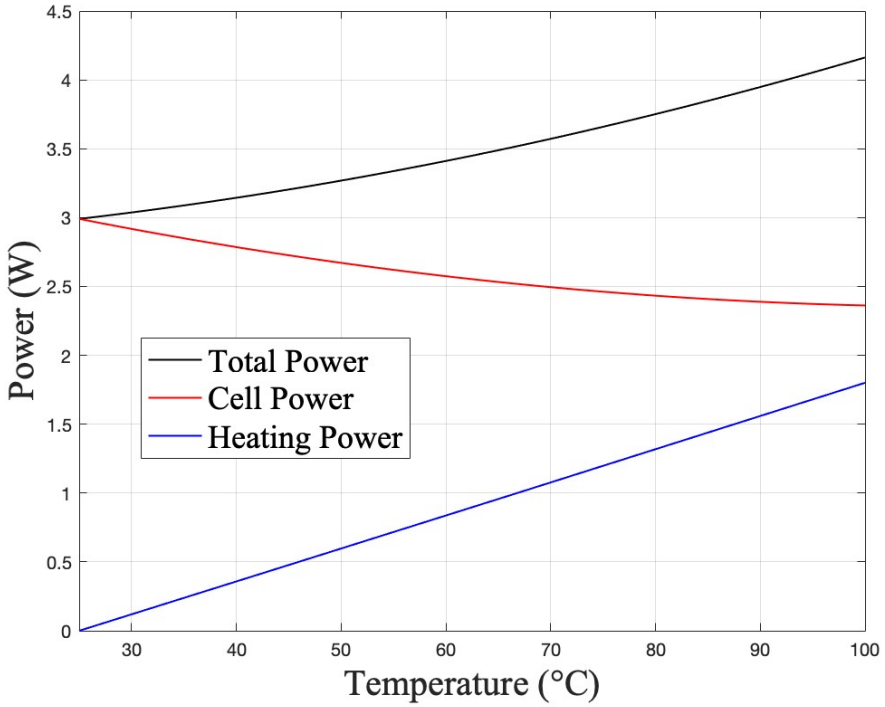

Figure 21. Total reactor power required per cell as a function of temperature

B. HIGH TEMPERATURE STEAM ELECTROLYSIS

It was assumed that direct heat transfer through a steam generator would be used to heat the water used HTSE. In this way, the maximum operating temperature was limited based on the potential outlet temperature of an LFR. The analysis was conducted with temperatures up to 700°C because LFRs have the potential to achieve such high temperatures if concerns about corrosion can be mitigated in the future. As the operating temperature of the LFR goes up, the production efficiency of the system would also go up. This is due to the increased efficiency of the energy conversion through the S-CO_2 Brayton Cycle and the decreased energy required for electrolysis.

Figure 22 shows the calculated Thermoneutral and Open Cell Voltage for high-temperature electrolysis methods. As in section A of this chapter, the Thermoneutral Voltage is relatively constant across the range of temperatures evaluated. It is noted that the required cell voltage is significantly less for higher operating temperatures than for PEM or AWE.

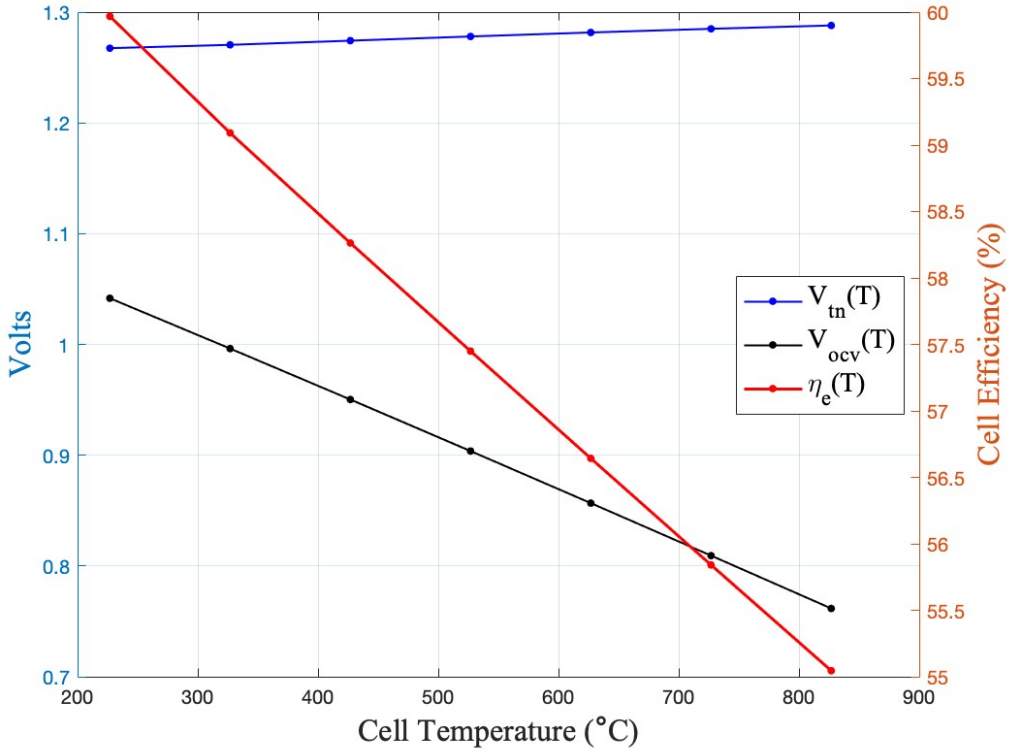

Figure 22. Thermoneutral voltage, open-circuit voltage, and cell efficiency vs. temperature for a HTSE cell

Using data from a study conducted on the performance of a proton-conducting SOEC [20], a polarization curve was created for temperatures of 600°C, 550°C, and 500°C. The results in Figure 23 show how the cell's current (I_{cell}) changes as a function of cell voltage (V_{cell}). Like the PEM material, there is less ohmic resistance for the cell at higher temperatures. Therefore, there is a higher I_{cell} for a given V_{cell} value at a higher temperature.

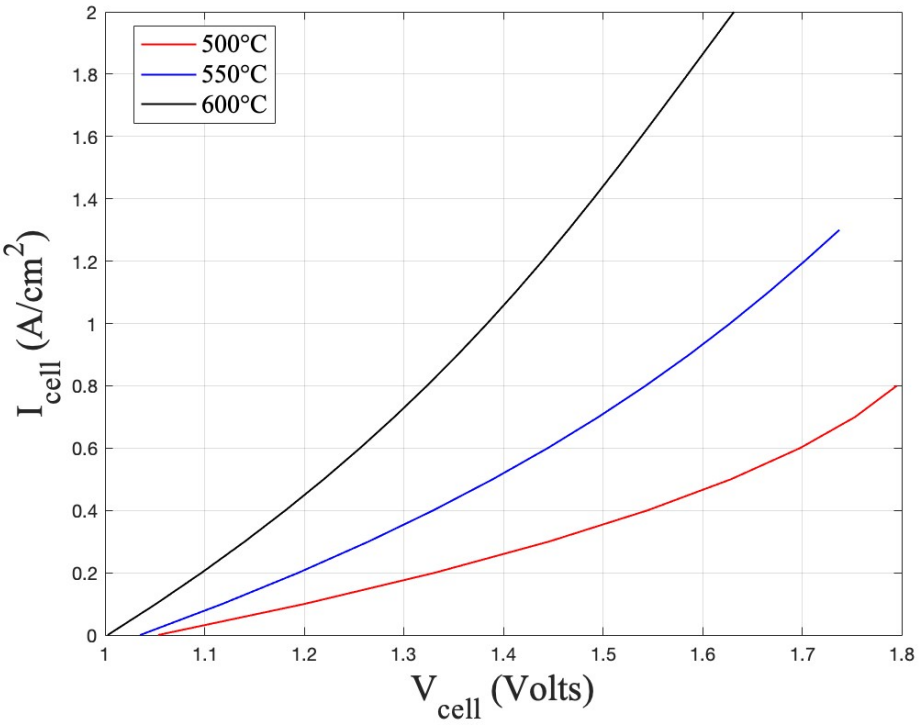

Figure 23. Polarization (aka I-V) plot for a P-SOEC. Adapted from [20].

The polarization data above was then used to determine a relationship between required cell voltage and percentage production increase as a function of temperature. This is demonstrated in Figure 24, where it was again assumed that the operating at a constant I_{cell} of .5 amps. As was expected, higher cell operating temperatures allow for greater cell production efficiency. However, the relationship is not linear and begins to plateau at temperatures higher than 650°C.

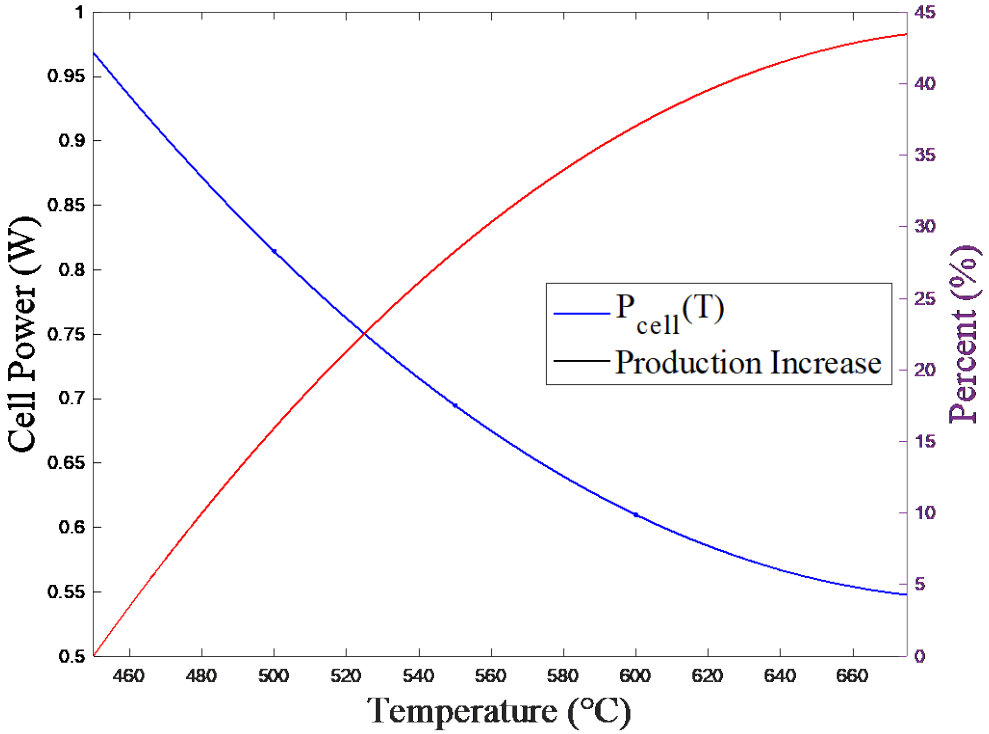

Figure 24. Required power and percent production increase as a function of cell temperature

The total reactor power required for HTSE was calculated. Because of the high temperatures required, it was assumed that a steam generator coupled directly to the primary fluid is used to heat the create the dry steam necessary for HTSE. An additional secondary loop using the S-CO_2 Brayton cycle would be used as the energy conversion method to meet all the electrical demands of the system. In this way, the operating temperature of the LFR had a direct effect on the production efficiency of the HTSE system. Figure 25 shows the reactor power required for electrolysis (Electrical Power) and power required to heat the water (Thermal Power) to cell operating temperatures. As is expected, the total reactor power required per cell (Total Power) goes down with operating temperature but levels off at temperatures greater than 660°.

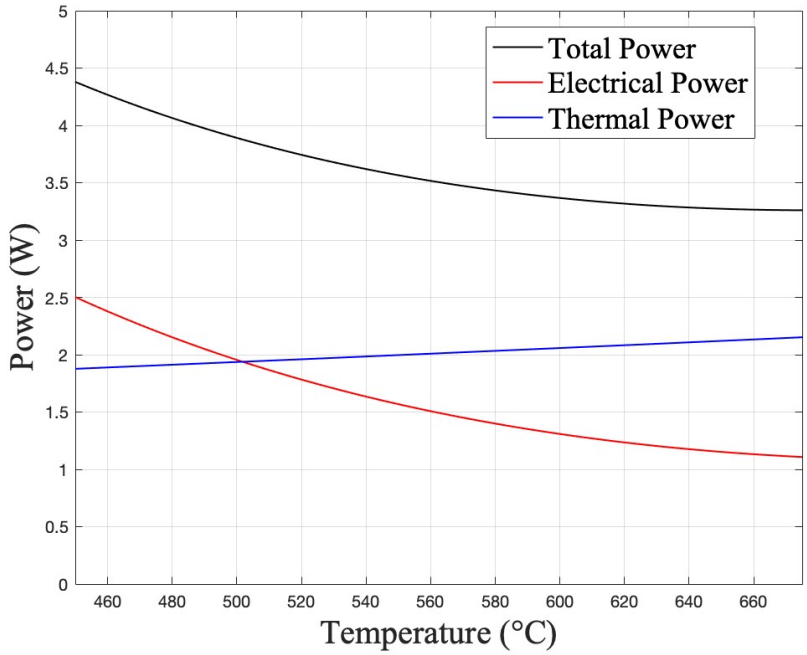

Figure 25. Thermal, electrical, and total power as a function of HTSE cell temperature

C. HYBRID THERMOCHEMICAL ELECTROLYSIS

Unlike the other electrolysis methods for water splitting, Hybrid Thermochemical Electrolysis methods require multiple stages to split the water molecule. The electricity required to force these reactions can be calculated by summing Gibbs's free energy change for the different reaction stages. For the modified sulfur-trioxide process described in Chapter II, Gibb's free Energy changes were calculated using NIST-JANAF Thermochemical Tables. The study [26] showed that the limiting reaction would be the Oxygen Evolution Reaction (OER) shown by eq. 2–12. The Thermoneutral voltage, Open-Circuit voltage, and cell efficiency for this reaction are shown in Figure 26 as a function of cell temperature.

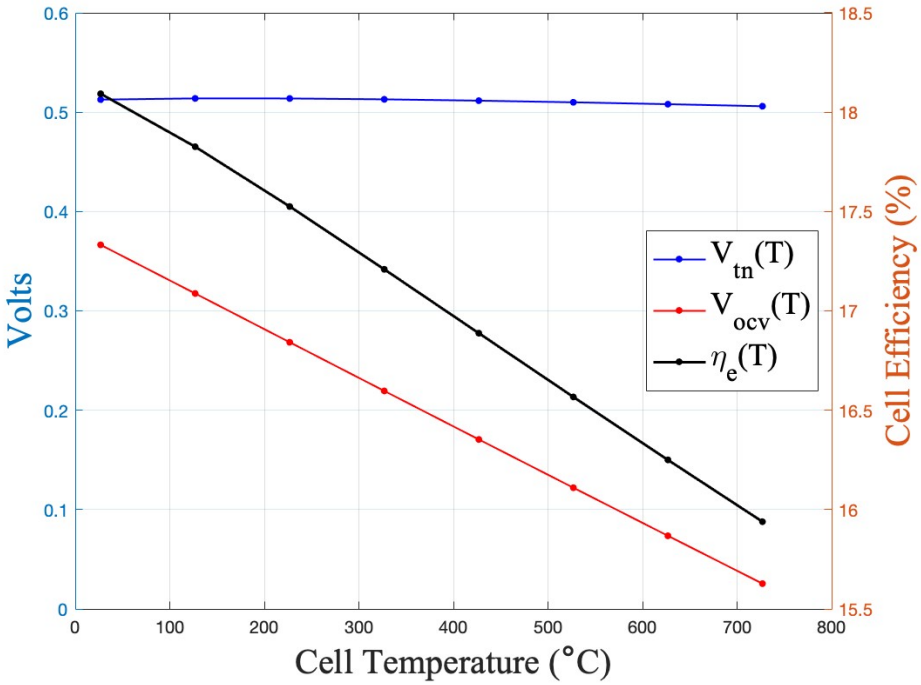

Figure 26. Thermoneutral voltage, open-circuit voltage, and cell efficiency vs. temperature for a hybrid cell

Because Hybrid Thermochemical Electrolysis is a relatively new area of research, there is limited experimental data on using sulfur trioxide electrolysis using a SOEC at high temperatures. This being the case, it was assumed for this analysis that ohmic resistance was constant across the range of temperatures analyzed. The reactor power required to provide the electricity (Electrical Power) and thermal Energy (Thermal Power) for the reaction was calculated and is shown in Figure 27. Interestingly, the total reactor power (Total Power) is relatively constant across the temperature range. As expected, the electricity needed goes down with temperature. It is also noted that significantly less electrical power is needed than the other water-splitting methods analyzed.

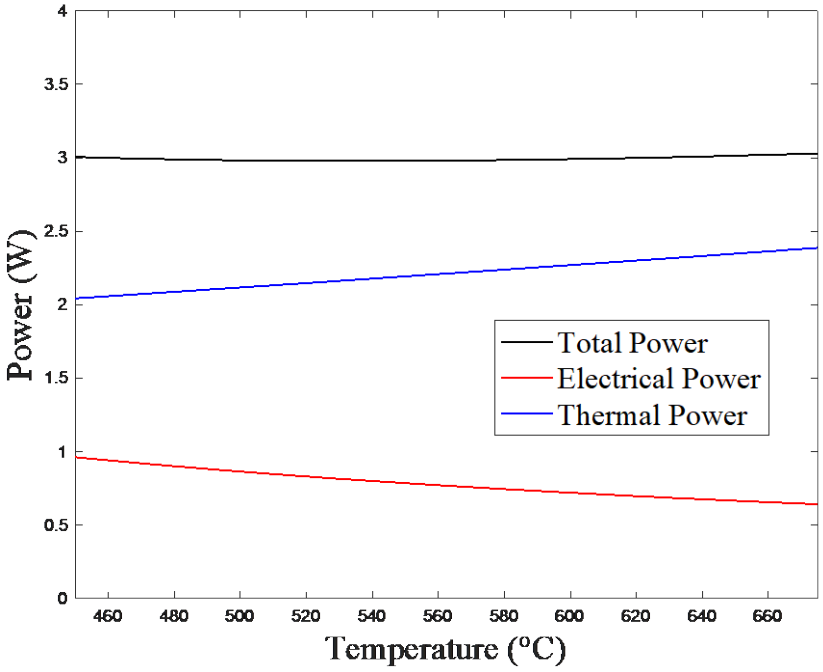

Figure 27. Thermal, electrical, and total power as a function of hybrid cell temperature

THIS PAGE INTENTIONALLY LEFT BLANK

VI. CONCLUSION/FOLLOW ON RESEARCH

Chapter V shows that the best means of hydrogen production with an LFR would be a Hybrid Thermochemical Electrolysis process. This is due to the lower power requirements for this process for a given production rate. Due to the limited testing conducted on hybrid electrolyzers, it is recommended that follow-up research be conducted on this process to determine the polarization properties of the cell materials used for this process.

Chapter V results also show that PEM electrolysis is an excellent alternative preferred over HTSE for hydrogen production. This was surprising because it was assumed that the reduced electrical energy required for the electrolysis reaction would reduce the total reactor power needed for the reaction. However, the high efficiency of the S-CO_2 Brayton cycle allowed reduced the burden of electrical demands enough to make the colder methods competitive with HTSE. This increased production efficiency coupled with the maturity, relative affordability, compactness, and durability of PEM technology make this method the best option for hydrogen production in an EABO environment using an LFR.

THIS PAGE INTENTIONALLY LEFT BLANK

APPENDIX A. MATLAB CODE

```
%% Thesis Final Analysis

%% Cell Data from Tables
close all
clear all

opts = spreadsheetImportOptions("NumVariables," 5);
opts.Sheet = ".1MPa_L";
opts.DataRange = "A6:E11";
opts.VariableNames = ["Tk," "Cp," "S," "DeltaH," "DeltaG"];
opts.VariableTypes = ["double," "double," "double," "double," "double"];
H2Ol = readtable("/Users/westonpatrick/Desktop/JANAF TABLE.xlsx," opts, "UseExcel,"
false);clear opts

opts = spreadsheetImportOptions("NumVariables," 5);
opts.Sheet = "1Bar";
opts.DataRange = "A11:E17";
opts.VariableNames = ["Tk," "Cp," "S," "DeltaH," "DeltaG"];
opts.VariableTypes = ["double," "double," "double," "double," "double"];
Bar1 = readtable("/Users/westonpatrick/Desktop/JANAF TABLE.xlsx," opts, "UseExcel," false);
clear opts

opts = spreadsheetImportOptions("NumVariables," 5);
opts.Sheet = "10Bar";
opts.DataRange = "A12:E18";
opts.VariableNames = ["Tk," "Cp," "S," "DeltaH," "DeltaG"];
opts.VariableTypes = ["double," "double," "double," "double," "double"];
Bar10 = readtable("/Users/westonpatrick/Desktop/JANAF TABLE.xlsx," opts, "UseExcel," false);
clear opts

opts = spreadsheetImportOptions("NumVariables," 5);
opts.Sheet = "100Bar";
opts.DataRange = "A4:E12";
opts.VariableNames = ["Tk," "Cp," "S," "DeltaH," "DeltaG"];
opts.VariableTypes = ["double," "double," "double," "double," "double"];
Bar100 = readtable("/Users/westonpatrick/Desktop/JANAF TABLE.xlsx," opts, "UseExcel," false);
clear opts

Effcell = .4;          % cell voltage
z = 2;                 % number of electrons
F = 96485;             % [C/mol] Faraday constant
R = 8.314;             % [Jdeg/Kmol] gas constant
H20 = 1;               % equals 1 for alkaline and PEM electrolysis
```

```
H2 = .5;              % concentration of H2
O2 = .5;              % concentration of O2

dH_H2Ol = -1000.*H2Ol.DeltaH;
dH_1Bar = -1000.*Bar1.DeltaH;
dH_10Bar = -1000.*Bar10.DeltaH;
dH_100Bar = -1000.*Bar100.DeltaH;

dG_H2Ol = -1000.*H2Ol.DeltaG;
dG_1Bar = -1000.*Bar1.DeltaG;
dG_10Bar = -1000.*Bar10.DeltaG;
dG_100Bar = -1000.*Bar100.DeltaG;

T_H2Ol = H2Ol.Tk;
T_1Bar = Bar1.Tk;
T_10Bar = Bar10.Tk;
T_100Bar = Bar100.Tk;

dS_H2Ol = (dH_H2Ol - dG_H2Ol)./T_H2Ol;
dS_1Bar = (dH_1Bar - dG_1Bar)./T_1Bar;
dS_10Bar = (dH_10Bar - dG_10Bar)./T_10Bar;
dS_100Bar = (dH_100Bar - dG_100Bar)./T_100Bar;

dQ_H2Ol = T_H2Ol.*dS_H2Ol;
dQ_1Bar = T_1Bar.*dS_1Bar;
dQ_10Bar = T_10Bar.*dS_10Bar;
dQ_100Bar = T_100Bar.*dS_100Bar;

Vtn_H2Ol = dH_H2Ol./(z*F);
Vtn_1Bar = dH_1Bar./(z*F);
Vtn_10Bar = dH_10Bar./(z*F);
Vtn_100Bar = dH_100Bar./(z*F);

Vrev_H2Ol = dG_H2Ol./(z*F);
Vrev_1Bar = dG_1Bar./(z*F);
Vrev_10Bar = dG_10Bar./(z*F);
Vrev_100Bar = dG_100Bar./(z*F);

Vocv_H2Ol =Vrev_H2Ol-(R.*T_H2Ol)./(z*F).*log(H20/(H2*O2^2));
Vocv_1Bar =Vrev_1Bar-(R.*T_1Bar)./(z*F).*log(H20/(H2*O2^2));
Vocv_10Bar =Vrev_10Bar-(R.*T_10Bar)./(z*F).*log(H20/(H2*O2^2));
Vocv_100Bar =Vrev_100Bar-(R.*T_100Bar)./(z*F).*log(H20/(H2*O2^2));

Vcell_H2Ol = 1.6;
Vcell_1Bar = 1.6;
Vcell_10Bar = 1.6;
Vcell_100Bar = 1.6;
```

```
Nloss_H2Ol = Vcell_H2Ol - Vrev_H2Ol;
Nloss_1Bar = Vcell_1Bar - Vrev_1Bar;
Nloss_10Bar = Vcell_10Bar - Vrev_10Bar;
Nloss_100Bar = Vcell_100Bar - Vrev_100Bar;

dQloss_H2Ol = z*F.*Nloss_H2Ol;
dQloss_1Bar = z*F.*Nloss_1Bar;
dQloss_10Bar = z*F.*Nloss_10Bar;
dQloss_100Bar = z*F.*Nloss_100Bar;

% Wir_H2Ol = dH_H2Ol+dQloss_H2Ol;
% Wir_1Bar = dH_1Bar+dQloss_1Bar;
% Wir_10Bar = dH_10Bar+dQloss_10Bar;
% Wir_100Bar = dH_100Bar+dQloss_100Bar;

Wir_H2Ol = z*F.*Vcell_H2Ol+dQloss_H2Ol;
Wir_1Bar = z*F.*Vcell_1Bar+dQloss_1Bar;
Wir_10Bar = z*F.*Vcell_10Bar+dQloss_10Bar;
Wir_100Bar = z*F.*Vcell_100Bar+dQloss_100Bar;

Effcell_H2Ol = dH_H2Ol./Wir_H2Ol;
Effcell_1Bar = dH_1Bar./Wir_1Bar;
Effcell_10Bar = dH_10Bar./Wir_10Bar;
Effcell_100Bar = dH_100Bar./Wir_100Bar;

% Effsys = .44*Effcell_H2Ol;

figure(1)
yyaxis left
% plot(T_1Bar-273.15,Vtn_1Bar,'-ob','LineWidth',1.0,'MarkerSize',8)
% plot(T_10Bar-273.15,Vtn_10Bar,'.-b','LineWidth',1.0,'MarkerSize',10)
plot(T_H2Ol-273.15,Vtn_H2Ol,'.-b','LineWidth',1.0,'MarkerSize',10)
hold on
% plot(T_1Bar-273.15,Vocv_1Bar,'-or','LineWidth',1.0,'MarkerSize',8)
% plot(T_10Bar-273.15,Vocv_10Bar,'.-k','LineWidth',1.0,'MarkerSize',10)
plot(T_H2Ol-273.15,Vocv_H2Ol,'.-b','LineWidth',1.0,'MarkerSize',10)

xlabel('Cell Temperature (\circC)','FontName','Times New Roman','FontSize',20)
ylabel('Volts','FontName','Times New Roman','FontSize',20)
grid on

yyaxis right
% plot(T_1Bar-273.15,100*Effcell_1Bar,'-ok','LineWidth',1.5,'MarkerSize',8)
% plot(T_10Bar-273.15,100*Effcell_10Bar,'.-r','LineWidth',1.5,'MarkerSize',10)
plot(T_H2Ol-273.15,100*Effcell_H2Ol,'.-r','LineWidth',1.5,'MarkerSize',10)
ylabel('Cell Efficiency (%)','FontName','Times New Roman','FontSize',20)
```

```
legend('V_t_n(T)','V_o_c_v(T)','\eta_e(T)','Location','east','FontName','Times New
Roman','FontSize',18)
%  legend('V_t_n, P = 1Bar','V_t_n, P = 10Bar', ...
%     'V_o_c_v, P = 1Bar', 'V_o_c_v, P = 10Bar', ...
%     '\eta_e, P = 1Bar','\eta_e, P = 10Bar','Location','southwest','FontName','Times New
Roman','FontSize',10)

% xline(80)
% plot(T_1Bar-273.15,Effcell_1Bar,'-*r')

% plot(T_H2Ol-273.15,Vrev_H2Ol,'-*k')
% hold on
% plot(T_H2Ol-273.15,Vtn_H2Ol,'-*b')
% plot(T_H2Ol-273.15,Vcell_H2Ol,'-*r')
% legend('V_r_e_v','V_t_n','V_c_e_l_l','Location','Best')

% plot(T_H2Ol,Vrev_H2Ol./Vtn_H2Ol)

% A_cell_1 = 4e4;                 % [cm^2] AWE cell area
% A_cell_2 = .03e4;               % [cm^2] PEM cell area
% I_1= .4e-3.*A_cell_1;           % [A] current AWE
% I_2= 2.0.*A_cell_2;             % [A] current PEM
%
% P_1 = 5.9.*760;                 % energy concumption per stack
% P_2 = 5.6.*10;                  % energy consumption per stack
%
% Pe_1 = Vrev_H2Ol.*I_1;          % [W]
% Pe_2 = Vrev_H2Ol.*I_2;          % [W]
% Prx = 19.8e6/5;                 % [W] Electrical power of reactor
%
% Vdot_1 = Prx./Pe_1;
% Vdot_2 = Prx./Pe_2;
%
% yyaxis right
% plot(T_H2Ol-273.15,Vdot_1.)
%
% yyaxis left
% plot(T_H2Ol-273.15,Vdot_2)

% Pratio_1 = (Vocv_H2Ol+1.2)./(Vocv_H2Ol(1)+1.2);
% Pratio_2 = (Vocv_H2Ol+1)./(Vocv_H2Ol(1)+1);
% yyaxis left
% plot (T_H2Ol-273.15,Pratio,'.-b')
% ylabel('Fraction of Energy Consumption')
%
% yyaxis right
```

```
% plot (T_H2Ol-273.15, 1./Pratio_1.*100-100,'.-b','LineWidth',1.5,'MarkerSize',10)
% hold on
% plot (T_H2Ol-273.15, 1./Pratio_2.*100-100,'.-r','LineWidth',1.5,'MarkerSize',10)
%
% ylabel('Production Increase (%)','FontName','Times New Roman','FontSize',16)
% xlabel('Cell temperature (\circC)','FontName','Times New Roman','FontSize',16)
% legend('Alkaline','PEM','location','Best','FontName','Times New Roman','FontSize',12)
% ylim([0 6])

%% PEM analysis
clear all
close all
opts = spreadsheetImportOptions("NumVariables," 5);
opts.Sheet = ".1MPa_L";
opts.DataRange = "A6:E11";
opts.VariableNames = ["Tk," "Cp," "S," "DeltaH," "DeltaG"];
opts.VariableTypes = ["double," "double," "double," "double," "double"];
H2Ol = readtable("/Users/westonpatrick/Desktop/JANAF TABLE.xlsx," opts, "UseExcel,"
false);clear opts

z = 2;              % number of electrons
F = 96485;          % [C/mol] Faraday constant
R = 8.314;          % [Jdeg/Kmol] gas constant
H20 = 1;            % equals 1 for alkaline and PEM electrolysis
H2 = .5;            % concentration of H2
O2 = .5;            % concentration of O2

dH_H2Ol = -1000.*H2Ol.DeltaH;
dG_H2Ol = -1000.*H2Ol.DeltaG;
T_H2Ol = H2Ol.Tk;
dS_H2Ol = (dH_H2Ol - dG_H2Ol)./T_H2Ol;
dQ_H2Ol = T_H2Ol.*dS_H2Ol;
Vtn_H2Ol = dH_H2Ol./(z*F);
Vrev_H2Ol = dG_H2Ol./(z*F);
Vocv_H2Ol =Vrev_H2Ol-(R.*T_H2Ol)./(z*F).*log(H20/(H2*O2^2));
Vcell_H2Ol = 1.6;
Nloss_H2Ol = Vcell_H2Ol - Vrev_H2Ol;
dQloss_H2Ol = z*F.*Nloss_H2Ol;
Wir_H2Ol = z*F.*Vcell_H2Ol+dQloss_H2Ol;
Effcell_H2Ol = dH_H2Ol./Wir_H2Ol;

figure(6)
yyaxis left
plot(T_H2Ol-273.15,Vtn_H2Ol,'.-b','LineWidth',1.0,'MarkerSize',10)

hold on
plot(T_H2Ol-273.15,Vocv_H2Ol,'.-r','LineWidth',1.0,'MarkerSize',10)
```

```
xlabel('Cell Temperature (\circC)','FontName','Times New Roman','FontSize',20)
ylabel('Volts','FontName','Times New Roman','FontSize',20)
grid on

yyaxis right
plot(T_H2Ol-273.15,100*Effcell_H2Ol,'.-k','LineWidth',1.5,'MarkerSize',10)
ylabel('Cell Efficiency (%)','FontName','Times New Roman','FontSize',20)
legend('V_t_n(T)','V_o_c_v(T)','\eta_e(T)','Location','east','FontName','Times New
Roman','FontSize',18)

% make polarization curve

close all
I_30r = [0    .025 .05  .1   .2   .4   .6   .8   1.0];
V_30r = [1.23 1.43 1.51 1.65 1.83 2.18 2.51 2.83 3.17];

I_40r = [0    .025 .05  .1   .2   .4   .6  .8  1.0];
V_40r = [1.23 1.42 1.49 1.6  1.77 2.1  2.4 2.7 2.96];

I_50r = [0    .025 .05  .1   .2   .4   .6  .8   1.0];
V_50r = [1.23 1.41 1.47 1.56 1.73 2.02 2.3 2.55 2.80];

I_60r = [0    .025 .05  .1   .2   .4   .6  .8   1.0];
V_60r = [1.23 1.41 1.47 1.55 1.70 1.95 2.2 2.42 2.65];

I_70r = [0    .025 .05  .1   .2   .4   .6   .8   1.0];
V_70r = [1.23 1.40 1.47 1.53 1.67 1.90 2.12 2.34 2.53];


figure(7)
plot(V_30r,I_50r,'-r','LineWidth',1.0,'MarkerSize',10)
hold on
plot(V_40r,I_50r,'-g','LineWidth',1.0,'MarkerSize',10)
plot(V_50r,I_50r,'-b','LineWidth',1.0,'MarkerSize',10)
plot(V_60r,I_50r,'-y','LineWidth',1.0,'MarkerSize',10)
plot(V_70r,I_50r,'-m','LineWidth',1.0,'MarkerSize',10)
ylabel('I_c_e_l_l (A/cm^2)','FontName','Times New Roman','FontSize',20)
xlabel('V_c_e_l_l (Volts)','FontName','Times New Roman','FontSize',20)
legend('30°C','40°C','50°C','60°C','70°C','Location','best','FontName','Times New
Roman','FontSize',14)
grid on

P_30 = polyfit(I_30r(4:9),V_30r(4:9),1);
P_40 = polyfit(I_40r(4:9),V_40r(4:9),1);
P_50 = polyfit(I_50r(4:9),V_50r(4:9),1);
P_60 = polyfit(I_60r(4:9),V_60r(4:9),1);
P_70 = polyfit(I_70r(4:9),V_70r(4:9),1);
```

```
I_cell= .1:.1:1.4;

V_30 = polyval(P_30,I_cell);
V_40 = polyval(P_40,I_cell);
V_50 = polyval(P_50,I_cell);
V_60 = polyval(P_60,I_cell);
V_70 = polyval(P_70,I_cell);

% % Plot data points and find best fit line.
% figure (8)
% plot(I_cell,V_30,'-r')
% hold on
% plot(I_cell,V_40,'-g')
% plot(I_cell,V_50,'-b')
% plot(I_cell,V_60,'-y')
% plot(I_cell,V_70,'-m')

% Find Power from P
P_el_30 = V_30.*I_cell;
P_el_40 = V_40.*I_cell;
P_el_50 = V_50.*I_cell;
P_el_60 = V_60.*I_cell;
P_el_70 = V_70.*I_cell;

z = 2;                  % number of electrons
F = 96485;              % [C/mol] Faraday constant
Eff_farad= .975;        % faradaic efficiency (current lost due to leakage) from 3-d ref
n_c = 10;               % number of electrolysis cells in a stack (guessed)
Vmol = 24.465e-3.*3600;     % molar volume of gas at 1atm and 25C

% % Find production rate from eq. 26 in "a critical review on the on def
Vdot_30 = Eff_farad.*n_c.*abs(I_cell)./(2.*F)*Vmol; % (Nm^3/hr)


% plot Power vs temperature
X = find(I_cell==.5);

P_cell = [P_el_30(X) P_el_40(X) P_el_50(X) P_el_60(X) P_el_70(X)];
T = [30 40 50 60 70];
P_cell_fit = polyfit(T,P_cell,2);

T_th = 25:100;
P_cell_th = polyval(P_cell_fit,T_th);

P_el_th = P_cell_th/.4;
```

```
% Plot P_cell vs Temerapture
figure(9)
yyaxis left
plot(T,P_cell,'.b','MarkerSize',8)
hold on
plot(T_th,P_cell_th,'-b','LineWidth',1.0)
xlabel('Temperature (°C)','FontName','Times New Roman','FontSize',20)
ylabel('Cell Power (W)','FontName','Times New Roman','FontSize',20)
yyaxis right
plot(T_th,100.*(1-P_cell_th./P_cell_th(1)),'-r','LineWidth',1.0)
legend('','P_c_e_l_l(T)','Production Increase','Location','east','FontName','Times New
Roman','FontSize',18)
ylabel('Percent (%)','FontName','Times New Roman','FontSize',20)
grid on

% Find power required to raise temperature to this value.
% Constant Values
C_steam = .2;               % Steam conversion rate. Graph Page 208
https://ebookcentral.proquest.com/lib/ebook-nps/reader.action?docID=1956440&ppg=280
M_H2 = 2.016e-3;            % (kg/mol) molar mass of Hydrogen.
V_H2 = 12.1;                % (Nm^3/kg)https://www.engineeringtoolbox.com/hydrogen-d_1419.html
M_H2O = 18.0158e-3;         % (kg/mol) molar mass of H20

% Find kg H20 needed
% N_H2 =  Vdot_30(find(X))./(3600.*V_H2.*M_H2); % (mol/sec) H2 production rate
N_H2 = 2.5337e-05;
N_H2O = N_H2./C_steam;              % (mol/sec) Mol H2O needed = 1:1 ratio divided by
conversion rate
m_H2O = M_H2O.*N_H2O;               % (kg/sec) mass of H2O needed

% Find power needed to raise temperature
Eff_SCO2 = .4;                      % assumed efficiency of SCO2
T_1Bar = H2Ol.Tk;
Cp_H2Ol = H2Ol.Cp;

% Q = Cp*N*dT  (given Cp is in j/(mol*k), N = moles, dT is change in T)

i = 1;
Q(1)=0;
while i <length(T_th)
  dT= T_th(i+1)-T_th(i);
  if T_th(i)<=26
     Cp_th = Cp_H2Ol(2);
  elseif T_th(i)>26 && T_th(i)<=46
     Cp_th = Cp_H2Ol(3);
  elseif T_th(i)>46 && T_th(i)<=66
     Cp_th = Cp_H2Ol(4);
```

```
  elseif T_th(i)>66 && T_th(i)<=86
     Cp_th = Cp_H2Ol(5);
  end
  Q(i+1) = Q(i) + N_H2O.*Cp_th.*dT;
  i = i+1;
end

Pth = Q./Eff_SCO2;                  % (W) thermal power needed per cell to raise temperature

Ptot = Pth +P_el_th;

figure(10)
plot(T_th,Ptot,'-k','LineWidth',1.0)
hold on
plot(T_th, P_el_th,'-r','LineWidth',1.0)
plot(T_th, Pth,'-b','LineWidth',1.0)
xlabel('Temperature (°C)','FontName','Times New Roman','FontSize',20)
ylabel('Power (W)','FontName','Times New Roman','FontSize',20)
legend('Total Power','Cell Power','Heating Power','Location','best','FontName','Times New
Roman','FontSize',18)
grid on
xlim([25 100])


%% HTSE

% Find Polarization plot
close all
clear all

I_600r = [-2.5  -1.8 -1.45 -1.1 -.74 -.42 -.21  0   .35 .7 .9];
V_600r = [1.75   1.6  1.5   1.4  1.3  1.2  1.1  1.0 .8  .6 .4];

I_550r = [-1.3  -1.0 -.71  -0.5 -0.3 -.23 -0.1  0    .25 .4 .6];
V_550r = [1.75   1.6  1.5   1.4  1.3  1.2  1.1  1.05 .8  .6 .4];

I_500r = [-0.7  -.45 -.35  -.25 -.20 -.10 -.05  0    .15 .25 .35];
V_500r = [1.75   1.6  1.5   1.4  1.3  1.2  1.1  1.1  .8  .6 .4];

P_600 = polyfit(I_600r,V_600r,3);
P_550 = polyfit(I_550r,V_550r,3);
P_500 = polyfit(I_500r,V_500r,3);

xfit_600= -2.5:.1:1;
xfit_550= -1.5:.1:.7;
xfit_500= -.7:.1:.5;
```

```
yfit_600 = polyval(P_600,xfit_600);
yfit_550 = polyval(P_550,xfit_550);
yfit_500 = polyval(P_500,xfit_500);

% % Plot data points and find best fit line.
% figure (1)
% plot(xfit_600,yfit_600,'-b')
% hold on
% plot(xfit_550,yfit_550,'-k')
% plot(xfit_500,yfit_500,'-r')

I_600 = -2.0:.1:0;
I_550 = -1.3:.1:0;
I_500 = -.8:.1:0;

V_600 = polyval(P_600,I_600);
V_550 = polyval(P_550,I_550);
V_500 = polyval(P_500,I_500);

P_el_600 = -V_600.*I_600;
P_el_550 = -V_550.*I_550;
P_el_500 = -V_500.*I_500;

z = 2;                  % number of electrons
F = 96485;              % [C/mol] Faraday constant
Eff_farad= .975;        % faradaic efficiency (current lost due to leakage) from 3-d ref
n_c = 10;               % number of electrolysis cells in a stack (guessed)
Vmol = 24.465e-3.*3600;     % molar volume of gas at 1atm and 25C

% Find production rate from eq. 26 in "a critical review on the on def
Vdot_600 = Eff_farad.*n_c.*abs(I_600)./(2.*F)*Vmol; % (Nm^3/hr)
Vdot_550 = Eff_farad.*n_c.*abs(I_550)./(2.*F)*Vmol; % (Nm^3/hr)
Vdot_500 = Eff_farad.*n_c.*abs(I_500)./(2.*F)*Vmol; % (Nm^3/hr)

Percent_600 = 100.*(Vdot_600./Vdot_600(1));
Percent_550 = 100.*(Vdot_550./Vdot_550(1));
Percent_500 = 100.*(Vdot_500./Vdot_500(1));

% Plot Voltage required to achieve a given current
figure(2)

plot(V_500,-I_500,'-r','LineWidth',1.0,'MarkerSize',10)
hold on
plot(V_550,-I_550,'-b','LineWidth',1.0,'MarkerSize',10)
plot(V_600,-I_600,'-k','LineWidth',1.0,'MarkerSize',10)
ylabel('I_c_e_l_l (A/cm^2)','FontName','Times New Roman','FontSize',20)
xlabel('V_c_e_l_l (Volts)','FontName','Times New Roman','FontSize',20)
```

```
legend('500°C','550°C','600°C','Location','best','FontName','Times New Roman','FontSize',14)
grid on

% Plot Cell power vs current
% figure(3)
% plot(-I_600,P_el_600,'-b','LineWidth',1.0)
% hold on
% plot(-I_550,P_el_550,'-k','LineWidth',1.0)
% plot(-I_500,P_el_500,'-r','LineWidth',1.0)
% xlim([0 1.3])
% ylim([0 1.6])
% xlabel('Cell Current (A)','FontName','Times New Roman','FontSize',16)
% ylabel('Cell Power (W)','FontName','Times New Roman','FontSize',16)
% legend('Tc = 600\circC','Tc = 550\circC','Tc = 500\circC','Location','best','FontName','Times
New Roman','FontSize',14)
% grid on

% plot Cell Power vs temperature
X_600 = find(I_600==-.5);
X_550 = find(I_550==-.5);
X_500 = find(I_500==-.5);

P_cell = [P_el_600(X_600) P_el_550(X_550) P_el_500(X_500)];
T = [600 550 500];
P_cell_fit = polyfit(T,P_cell,2);

T_th = 450:700;
P_cell_th = polyval(P_cell_fit,T_th);

% Find eff of S-CO2 Brayton cycle based on temperature:
T_SCO2 = [360 390 440 495 550 602 655 702 750 805 860];
Eff_SCO2 = 1e-2.*[32.6 34.8 38.0 41.4 44.3 46.8 48.6 50.2 51.7 52.4 53.1];

P = polyfit(T_SCO2,Eff_SCO2,4);
Eff_SCO2 = polyval(P,T_th);

% Find electrical power based on data above
P_el_th = P_cell_th./Eff_SCO2;

% figure(4)
yyaxis left
plot(T,P_cell,'.b','MarkerSize',8)
hold on
plot(T_th,P_cell_th,'-b','LineWidth',1.0)
xlabel('Temperature (°C)','FontName','Times New Roman','FontSize',20)
ylabel('Cell Power (W)','FontName','Times New Roman','FontSize',20)
yyaxis right
```

```
plot(T_th,100.*(1-P_cell_th./P_cell_th(1)),'-r','LineWidth',1.0)
legend('','P_c_e_l_l(T)','Production Increase','Location','east','FontName','Times New
Roman','FontSize',18)
ylabel('Percent (%)','FontName','Times New Roman','FontSize',20)
xlim([450 675])
grid on

% Find power needed to raise temperature of water to steam

opts = spreadsheetImportOptions("NumVariables," 5);
opts.Sheet = "1Bar";
opts.DataRange = "A4:E16";
opts.VariableNames = ["Tk," "Cp," "S," "DeltaH," "DeltaG"];
opts.VariableTypes = ["double," "double," "double," "double," "double"];
Bar1 = readtable("/Users/westonpatrick/Desktop/JANAF TABLE.xlsx," opts, "UseExcel," false);
clear opts

% Find power required to raise temperature to this value.
% Constant Values
C_steam = 1;              % Steam conversion rate. Graph Page 208
https://ebookcentral.proquest.com/lib/ebook-nps/reader.action?docID=1956440&ppg=280
M_H2 = 2.016e-3;          % (kg/mol) molar mass of Hydrogen.
V_H2 = 12.1;              % (Nm^3/kg)https://www.engineeringtoolbox.com/hydrogen-d_1419.html
M_H2O = 18.0158e-3;       % (kg/mol) molar mass of H20

% Find kg H20 needed
N_H2 =  Vdot_600(find(I_600==-.5))./(3600.*V_H2.*M_H2); % (mol/sec) H2 production rate
N_H2O = N_H2./C_steam;            % (mol/sec) Mol H2O needed = 1:1 ratio divided by
conversion rate
m_H2O = M_H2O.*N_H2O;             % (kg/sec) mass of H2O needed

% Find power needed to raise temperature
Eff_hx = .9;                      % assumed efficiency of HX
T_1Bar = Bar1.Tk;
Cp_1Bar = Bar1.Cp;

% Q = Cp*N*dT  (given Cp is in j/(mol*k), N = moles, dT is change in T)
Q = 40.8e3.*N_H2O;        %(J/sec aka Watt) Energy of transition from liquid to steam. ( =m*dHf)
for i = 1:9
  dT= T_1Bar(i+1)-T_1Bar(i);
  Q = Q + N_H2O.*Cp_1Bar(i+1).*dT;
end

i = 1;
Q(1) = Q;
while i <length(T_th)
  dT= T_th(i+1)-T_th(i);
```

```
  if T_th(i)<=426
     Cp_th = Cp_1Bar(9);
  elseif T_th(i)>426 && T_th(i)<=526
     Cp_th = Cp_1Bar(10);
  elseif T_th(i)>526 && T_th(i)<=626
     Cp_th = Cp_1Bar(11);
  elseif T_th(i)>626 && T_th(i)<=726
     Cp_th = Cp_1Bar(12);
  end
  Q(i+1) = Q(i) + N_H2O.*Cp_th.*dT;
  i = i+1;
end

Pth = Q./Eff_hx;                % (W) thermal power needed per cell to raise temperature

Ptot = Pth +P_el_th;

figure(5)
plot(T_th,Ptot,'-k','LineWidth',1.0)
hold on
plot(T_th, P_el_th,'-r','LineWidth',1.0)
plot(T_th, Pth,'-b','LineWidth',1.0)
xlabel('Temperature (°C)','FontName','Times New Roman','FontSize',20)
ylabel('Power (W)','FontName','Times New Roman','FontSize',20)
ylim([0 5])
xlim([450 675])
legend('Total Power','Electrical Power','Thermal Power','Location','best','FontName','Times New
Roman','FontSize',18)
grid on

%% Hybrid Reaction
clear all
close all

opts = spreadsheetImportOptions("NumVariables," 7);
opts.Sheet = "SO3";
opts.DataRange = "B25:H32";
opts.VariableNames = ["Tk," "Cp," "S," "DeltaH," "DeltaG," "VarName7," "TC"];
opts.VariableTypes = ["double," "double," "double," "double," "double," "double," "double"];
SO3 = readtable("/Users/westonpatrick/Desktop/JANAF TABLE.xlsx," opts, "UseExcel," false);
clear opts

opts = spreadsheetImportOptions("NumVariables," 5);
opts.Sheet = "1Bar";
opts.DataRange = "A19:E26";
opts.VariableNames = ["Tk," "Cp," "S," "DeltaH," "DeltaG"];
opts.VariableTypes = ["double," "double," "double," "double," "double"];
```

```
Bar1 = readtable("/Users/westonpatrick/Desktop/JANAF TABLE.xlsx," opts, "UseExcel," false);
clear opts

Effcell = .4;          % cell voltage
z = 2;                % number of electrons
F = 96485;             % [C/mol] Faraday constant
R = 8.314;             % [Jdeg/Kmol] gas constant
H20 = 1;               % equals 1 for alkaline and PEM electrolysis
H2 = .5;              % concentration of H2
O2 = .5;              % concentration of O2

dH_SO3 = -1000.*SO3.DeltaH;
dG_SO3 = -1000.*SO3.DeltaG;
T_SO3 = SO3.Tk;
dS_SO3 = (dH_SO3 - dG_SO3)./T_SO3;
dQ_SO3 = T_SO3.*dS_SO3;
Vtn_SO3 = dH_SO3./(z*F);
Vrev_SO3 = dG_SO3./(z*F);
Vocv_SO3 = Vrev_SO3-(R.*T_SO3)./(z*F).*log(H20/(H2*O2^2));
Vcell_SO3 = 1.6;
Nloss_SO3 = Vcell_SO3 - Vrev_SO3;
dQloss_SO3 = z*F.*Nloss_SO3;
Wir_SO3 = z*F.*Vcell_SO3+dQloss_SO3;
Effcell_SO3 = dH_SO3./Wir_SO3;

figure(11)
yyaxis left
plot(T_SO3-273.15,Vtn_SO3,'.-b','LineWidth',1.0,'MarkerSize',10)
hold on
plot(T_SO3-273.15,Vrev_SO3,'.-r','LineWidth',1.0,'MarkerSize',10)
xlabel('Cell Temperature (\circC)','FontName','Times New Roman','FontSize',20)
ylabel('Volts','FontName','Times New Roman','FontSize',20)
grid on

yyaxis right
plot(T_SO3-273.15,100*Effcell_SO3,'.-k','LineWidth',1.5,'MarkerSize',10)
ylabel('Cell Efficiency (%)','FontName','Times New Roman','FontSize',20)
legend('V_t_n(T)','V_o_c_v(T)','\eta_e(T)','Location','east','FontName','Times New
Roman','FontSize',18)

dG_SO2 = 1000.*87.3;
Vrev_SO2 = dG_SO2./(z*F);

I = .5;
P_SO3 = Vrev_SO3.*I;
P_SO2 = Vrev_SO2.*I;
```

```
P_cell = P_SO2+P_SO3;

% figure(12)
% plot(T_SO3-273.15,P_el_data)
% xlabel('Temperature (°C)','FontName','Times New Roman','FontSize',20)
% ylabel('Power (W)','FontName','Times New Roman','FontSize',20)
% legend('Total Power','Electrical Power','Thermal Power','Location','best','FontName','Times
New Roman','FontSize',18)
% grid on

% Find power required to raise temperature to this value.

T_th = 450:675;

% Find eff of S-CO2 Brayton cycle based on temperature:
T_SCO2 = [360 390 440 495 550 602 655 702 750 805 860];
Eff_SCO2 = 1e-2.*[32.6 34.8 38.0 41.4 44.3 46.8 48.6 50.2 51.7 52.4 53.1];

P = polyfit(T_SCO2,Eff_SCO2,4);
Eff_SCO2 = polyval(P,T_th);

% Find electrical power based on data above
P_cell_fit = polyfit(T_SO3,P_cell, 1);
P_cell_th = polyval(P_cell_fit,T_th);
P_el_th = P_cell_th./Eff_SCO2;

% Find thermal power based on using heat exchanger to raise temperature
% Constant Values
C_steam = .8;               % Steam conversion rate. Graph Page 208
https://ebookcentral.proquest.com/lib/ebook-nps/reader.action?docID=1956440&ppg=280
M_H2 = 2.016e-3;            % (kg/mol) molar mass of Hydrogen.
V_H2 = 12.1;                % (Nm^3/kg)https://www.engineeringtoolbox.com/hydrogen-d_1419.html
M_H2O = 18.0158e-3;         % (kg/mol) molar mass of H20

% Find kg H20 needed
N_H2 =  2.5337e-05; % (mol/sec) H2 production rate
N_H2O = N_H2./C_steam;              % (mol/sec) Mol H2O needed = 1:1 ratio divided by
conversion rate
m_H2O = M_H2O.*N_H2O;               % (kg/sec) mass of H2O needed

% Find power needed to raise temperature
Eff_hx = .8;                        % assumed efficiency of HX
T_1Bar = Bar1.Tk;
Cp_1Bar = Bar1.Cp;

% Q = Cp*N*dT  (given Cp is in j/(mol*k), N = moles, dT is change in T)
Q = 40.8e3.*N_H2O;          %(J/sec aka Watt) Energy of transition from liquid to steam. ( =m*dHf)
```

```
for i = 1:3
  dT= T_1Bar(i+1)-T_1Bar(i);
  Q = Q + N_H2O.*Cp_1Bar(i+1).*dT;
end

i = 1;
Q(1) = Q;
while i <length(T_th)
  dT= T_th(i+1)-T_th(i);
  if T_th(i)<=426
     Cp_th = Cp_1Bar(4);
  elseif T_th(i)>426 && T_th(i)<=526
     Cp_th = Cp_1Bar(5);
  elseif T_th(i)>526 && T_th(i)<=626
     Cp_th = Cp_1Bar(6);
  elseif T_th(i)>626 && T_th(i)<=726
     Cp_th = Cp_1Bar(7);
  end
  Q(i+1) = Q(i) + N_H2O.*Cp_th.*dT;
  i = i+1;
end

Pth = Q./Eff_hx;                % (W) thermal power needed per cell to raise temperature

Ptot = Pth + P_el_th;

figure(13)
plot(T_th,Ptot,'-k','LineWidth',1.0)
hold on
plot(T_th, P_el_th,'-r','LineWidth',1.0)
plot(T_th, Pth,'-b','LineWidth',1.0)
xlabel('Temperature (°C)','FontName','Times New Roman','FontSize',20)
ylabel('Power (W)','FontName','Times New Roman','FontSize',20)
ylim([0 4])
xlim([450 675])
legend('Total Power','Electrical Power','Thermal Power','Location','best','FontName','Times New
Roman','FontSize',18)
grid on
```

APPENDIX B. NIST-JANAF THERMOCHEMICAL TABLES

Source: [49]

$H_2O_1(l)$

Water (H_2O)

Enthalpy Reference Temperature = T_r = 298.15 K Standard State Pressure = $p°$ = 0.1 MPa

		J·K^{-1} mol^{-1}			kJ·mol^{-1}		
***T*/K**	$C_p°$	$S°$	$-[G°-H°(T_r)]/T$	$H-H°(T_r)$	$\Delta_f H°$	$\Delta_f G°$	**log K$_f$**
0							
100							
200							
280	75.563	65.215	70.102	-1.368	-286.410	-240.123	44.796
298.15	75.351	69.950	69.950	0.	-285.830	-237.141	41.546
300	75.349	70.416	69.952	0.139	-285.771	-236.839	41.237
320	75.344	75.279	70.134	1.646	-285.137	-233.598	38.131
340	75.388	79.847	70.573	3.153	-284.506	-230.396	35.396
360	75.679	84.164	71.209	4.664	-283.874	-227.231	32.970
372.780	75.962	86.808	71.699	5.633	LIQUID <--> REAL GAS		
380	76.154	88.267	72.000	6.182	283.237	224.102	30.805
400	76.770	92.189	72.912	7.711	-282.591	-221.006	28.860
420	77.547	95.952	73.920	9.254	-281.934	-217.943	27.105
440	78.543	99.582	75.004	10.814	-281.262	-214.912	25.513

460	79.793	103.100	76.150	12.397	-280.569	-211.911	24.063
480	81.463	106.530	77.344	14.009	-279.850	-208.941	22.737
500	83.694	109.898	78.579	15.659	-279.095	-206.002	21.521

PREVIOUS: March 1979 (1 atm)

CURRENT: March 1979 (1 bar)

Water (H_2O)

$H_2O_1(l)$

Water, 1 Bar (H_2O) H_2O_1(l,g)

Enthalpy Reference Temperature = T_r = 298.15 K Standard State Pressure = $p°$ = 0.1 MPa

	J·K^{-1} mol^{-1}				kJ·mol^{-1}		
T/K	$C_p°$	$S°$	$-[G°-H°(T_r)]/T$	$H-H°(T_r)$	$\Delta_f H°$	$\Delta_f G°$	log K_f
0							
100							
200							
280	75.563	65.215	70.102	-1.368	-286.410	-240.123	44.796
298.15	75.351	69.950	69.950	0.	-285.830	-237.141	41.546
300	75.349	70.416	69.952	0.139	-285.771	-236.839	41.237
320	75.344	75.279	70.134	1.646	-285.137	-233.598	38.131
340	75.388	79.847	70.573	3.153	-284.506	-230.396	35.396
360	75.679	84.164	71.209	4.664	-283.874	-227.231	32.970
372.780	75.962	86.808	71.699	5.633	LIQUID <--> REAL GAS		
372.780	36.800	195.911	71.699	46.304	PRESSURE = 1 bar		
400	35.982	198.473	80.240	47.293	-243.009	-223.937	29.243
500	35.699	206.428	104.712	50.858	-243.896	-219.069	22.886
600	36.521	213.003	122.227	54.466	-244.797	-214.018	18.632
700	37.596	218.712	135.612	58.170	-245.658	-208.819	15.582
800	38.780	223.809	146.323	61.988	-246.461	-203.501	13.287
900	40.023	228.448	155.194	65.928	-247.198	-198.086	11.497

1000	41.292	232.730	162.736	69.994	-247.868	-192.593	10.060
1100	42.554	236.725	169.283	74.186	-248.468	-187.035	8.882
1200	43.781	240.481	175.061	78.504	-249.004	-181.426	7.897
1300	44.954	244.032	180.231	82.941	-249.479	-175.775	7.063

Water, 10 Bar (H_2O) H_2O_1(l,g)

Enthalpy Reference Temperature = T_r = 298.15 K Standard State Pressure = $p°$ = 0.1 MPa

	J·K^{-1} mol^{-1}				kJ·mol^{-1}		
T/K	$C_p°$	$S°$	$-[G°-H°(T_r)]/T$	$H-H°(T_r)$	$\Delta_f H°$	$\Delta_f G°$	log K_f
0							
100							
200							
298.15	75.313	69.946	69.946	0.	-285.815	-237.125	41.543
300	75.314	70.412	69.948	0.139	-285.756	-236.823	41.235
400	76.732	92.173	72.906	7.707	-282.580	-220.989	28.858
453.070	79.322	101.872	75.740	11.840	LIQUID <--> REAL GAS		
453.070	46.063	181.988	75.740	48.138	PRESSURE = 10 bar		
500	41.002	186.240	85.919	50.160	-244.579	-209.657	21.903
600	38.430	193.409	103.261	54.089	-245.159	-202.623	17.640
700	38.527	199.326	116.572	57.927	-245.886	-195.477	14.587
800	39.310	204.517	127.247	61.816	-246.618	-188.225	12.290
900	40.357	209.206	136.097	65.798	-247.314	-180.884	10.498
1000	41.517	213.517	143.626	69.891	-247.955	-173.468	9.061
1100	42.714	217.531	150.164	74.103	-248.537	-165.990	7.882
1200	43.900	221.298	155.937	78.434	-249.059	-158.462	6.898

1300	45.045	224.858	161.103	82.881	-249.524	-150.893	6.063
1400	46.134	228.236	165.778	87.441	-249.935	-143.291	5.346
1500	47.155	231.454	170.050	92.106	-250.299	-135.660	4.724

Sulfur Trioxide (SO_3) $O_3S_1(g)$

Enthalpy Reference Temperature = T_r = 298.15 K Standard State Pressure = $p°$ = 0.1 MPa

	J·K^{-1} mol^{-1}			kJ·mol^{-1}			
	$C_p°$	$S°$	$-[G°-H°(T_r)]/T$	$H-H°(T_r)$	$\Delta_f H°$	$\Delta_f G°$	log K_f
0	0.	0.	INFINITE	-11.697	-390.025	-390.025	INFINITE
100	34.076	212.371	295.976	-8.361	-391.735	-385.724	201.481
200	42.336	238.259	261.145	-4.577	-393.960	-378.839	98.943
250	46.784	248.192	257.582	-2.348	-394.937	-374.943	78.340
298.15	50.661	256.769	256.769	0.	-395.765	-371.016	65.000
300	50.802	257.083	256.770	0.094	-395.794	-370.862	64.573
350	54.423	265.191	257.402	2.726	-396.543	-366.646	54.719
400	57.672	272.674	258.849	5.530	-399.412	-362.242	47.304
450	60.559	279.637	260.777	8.487	-400.656	-357.529	41.501
500	63.100	286.152	262.992	11.580	-401.878	-352.668	36.843
600	67.255	298.041	267.862	18.107	-403.675	-342.647	29.830
700	70.390	308.655	272.945	24.997	-405.014	-332.365	24.801
800	72.761	318.217	278.017	32.160	-406.068	-321.912	21.019
900	74.570	326.896	282.973	39.531	-460.062	-310.258	18.007
1000	75.968	334.828	287.768	47.060	-459.581	-293.639	15.338
1100	77.065	342.122	292.382	54.714	-459.063	-277.069	13.157
1200	77.937	348.866	296.811	62.466	-458.521	-260.548	11.341
1300	78.639	355.133	301.060	70.296	-457.968	-244.073	9.807
1400	79.212	360.983	305.133	78.189	-457.413	-227.640	8.493
1500	79.685	366.465	309.041	86.135	-456.863	-211.247	7.356

Sulfur Dioxide (SO_2) $O_2S_1(g)$

Enthalpy Reference Temperature = T_r = 298.15 K

Standard State Pressure = $p°$ = 0.1 MPa

	J·K^{-1} mol^{-1}			kJ·mol^{-1}			
***T*/K**	C_p°	S°	$-[G^\circ - H^\circ(T_r)]/T$	$H - H^\circ(T_r)$	$\Delta_f H^\circ$	$\Delta_f G^\circ$	**log K$_f$**
0	0.000	0.000	INFINITE	-10.552	-294.299	-294.299	INFINITE
100	33.526	209.025	281.199	-7.217	-294.559	-296.878	155.073
200	36.372	233.033	251.714	-3.736	95.631	-298.813	78.042
298.15	39.878	248.212	248.212	0.000	-296.842	-300.125	52.581
300	39.945	248.459	248.213	0.074	-296.865	-300.145	52.260
400	43.493	260.448	249.824	4.250	-300.257	-300.971	39.303
500	46.576	270.495	252.979	8.758	-302.736	-300.871	31.432
600	49.049	279.214	256.641	13.544	-304.694	-300.305	26.144
700	50.961	286.924	260.427	18.548	-306.291	-299.444	22.345
800	52.434	293.829	264.178	23.721	-307.667	-298.370	19.482
900	53.580	300.073	267.825	29.023	-362.026	-296.051	17.182
1000	54.484	305.767	271.339	34.428	-361.940	-288.725	15.081
1100	55.204	310.995	274.710	39.914	-361.835	-281.409	13.363
1200	55.794	315.824	277.937	45.464	-361.720	-274.102	11.931
1300	56.279	320.310	281.026	51.069	-361.601	-266.806	10.720

1400	56.689	324.496	283.983	56.718	-361.484	-259.518	9.683
1500	57.036	328.419	286.816	62.404	-361.372	-252.239	8.784

THIS PAGE INTENTIONALLY LEFT BLANK

LIST OF REFERENCES

[1] R. O'Rourke, "Renewed Great Power Competition: Implications for Defense," 10 March 2022. [Online]. Available: https://crsreports.congress.gov/product/pdf/R/R43838. [Accessed 1st April 2022].

[2] Department of the Navy, "Tentative Manual For Expeditionary Advanced Base Operations," February 2021. [Online]. Available: https://www.mcwl.marines.mil/TMEABO/

[3] J. M. Richardson, "A Design For Maintaining Maritime Superiority," Defense.gov, Washington, D.C, 2018. [Online]. Available: https://media.defense.gov/2020/May/18/2002301999/-1/-1/1/DESIGN_2.0.PDF

[4] A. B. De la Rose, "Fischer-Tropsch Catalyst for Aviation Fuel Production," National Aeronautics and Space Administration, Glenn Research Center, Cleveland, Ohio, 2012. [Online]. Available: https://pdfs.semanticscholar.org/8f49/0ae4dbaa00a1fb9a33555b7bb809e1431359.pdf

[5] M. E. Dry, "The Fischer-Tropsch Process: 1950–2000," *Catalysis Today,* vol. 71, no. 3–4, pp. 227–241, 2002. [Online]. Available: https://doi.org/10.1016/S0920-5861(01)00453-9

[6] P. M. Maitlis and A. d. Klerk, *Greener Fischer-Tropsch Processes: For Fuels and Feedstocks*, Somerset: John Wiley & Sons, Incorporated, 2013 [Online]. Available: ProQuest

[7] H. D. Willauer, M. J. Bradley, J. W. Baldwin, J. J. Hartvigsen, L. Frost, J. R. Morse and D. J. Hasler, "Evaluation of Hydrogenation in a Modular Fixed-Bed Reactor Prototype," *Catalysts,* vol. 10, no. 9, p. 970, 2020. [Online]. Available: https://doi.org/10.3390/catal10090970

[8] M. Melaina and J. Eichman, "Hydrogen Energy Storage: Grid and Transportation Services," National Renewable energy Laboratory, Sacramento, CA, 2015. Available: ProQuest

[9] S. Kharel, and B. Shabani, "Hydrogen as a long-term, large-scale energy storage solution to support renewables," *Energies,* vol. 11, no. 10, 2018. [Online]. Available: https://doi.org/10.3390/en11102825

[10] “GEN IV International Forum,” 19 09 2013. [Online]. Available: https://www.gen-4.org/gif/jcms/c_40368/benefits-and-challenges#c_43122. [Accessed 04 04 2022].

[11] B. Hatala, A. Alemberti, S. Bourg, Y. Huang, F. Serre and M. A. Futtere, “GIF 2020 Annual Report,” GEN IV International Forum. [Online]. Available: https://www.gen-4.org/gif/jcms/c_44720/annual-reports

[12] I. Dincer, “Green methods for hydrogen production,” *International Journal of Hydrogen Energy,* vol. 37, no. 2, pp. 1954–1971, 2012. [Online]. Available: https://doi.org/10.1016/j.ijhydene.2011.03.173

[13] M. Yu, E. Budiyanto and H. Tuysuz, “Principles of Water Electrolysis and Recent Progress in Cobalt-, Nickel-, and Iron-Based Oxides for the Oxygen Evolution Reaction,” *Angewandte Chemie International Edition,* vol. 61, no. 1, 2021. [Online]. Available: https://doi.org/10.1002/anie.202103824

[14] K. W. Harrison, R. Remick, G. D. Martin and A. Hoskin, “Hydrogen Production: Fundamentals and Case Study Summaries,” in *18th World Hydrogen Energy Conference*, Essen, Germany, 2010. [Onlinef]. Available: https://www.nrel.gov/docs/fy10osti/48269.pdf

[15] A. Godula-Jopek, *Hydrogen Production: By Electrolysis*, Weinheim, Germany: John Wiley & Sons, Incorporated, 2015. [Online]. Available: ProQuest

[16] S. Marini, P. Salvi, P. Nelli, R. Pesenti, M. Villa, M. Berrettoni, G. Zangari and Y. Kiros, “Advanced Alkaline Water Electrolysis,” *Electrochimica Acta,* vol. 82, pp. 384–391, 2012. [Online]. Available: https://doi.org/10.1016/j.electacta.2012.05.011

[17] X. Yan and R. Hino, *Nuclear Hydrogen Production Handbook*, Boca Raton, FL: CRC Press, Taylor and Francis Group, 2011. [Online]. Available: https://doi.org/10.1201/b10789

[18] M. Carmo, D. L. Fritz, J. Mergel and D. Stolten, “A comprehensive review on PEM water Electrolysis,” *Hydrogen Energy,* vol. 38, pp. 4901–4934, 2013. [Online]. Available: https://doi.org/10.1016/j.ijhydene.2013.01.151

[19] F. Xue, J. Su, P. Li and Y. Zhang, “Application of Proton Exchange Membrane Electrolysis of Water Hydrogen Production Technology in Power Plant,” *IOP conference series. Earth and Environmental Science,* vol. 631, no. 1, p. 12079, 2021. [Online]. Available: https://iopscience.iop.org/article/10.1088/1755-1315/631/1/012079/pdf

[20] W. Wu, H. Ding, Y. Zhang, Y. Ding, P. Katiyar, P. K. Majumdar, T. He and D. Ding, "3D Self-Archtictured Steam Electrode Enabled Efficient and Durable Hydrogen Production in a Proton-Conducting Solid Exoide Electrolysis Cell at Temperatures Lower than 600C," *Advanced Science,* vol. 5, no. 11, p. 1800360, 2018. [Online]. Available: https://doi.org/10.1002/advs.201800360

[21] Z. Wang, M. Mori and T. Araki, "Steam electrolysis performance of intermediate-temperature solid oxide electrolysis cell and efficiency of hydrogen production system at 300 Nm," *International Journal of Hydrogen Energy,* vol. 35, pp. 4451–4458, 2010. [Online]. Available: https://doi.org/10.1016/j.ijhydene.2010.02.058

[22] G. Tao and A. Virkar, "A Reversible Planar Solid Oxide Fuel-Assisted Electrolysis Cell and Solid Oxide Fuel Cell for Hydrogen and Electricity Production Operating on Natural Gas/Biogas," DOE Hydrogen Program, Salt Lake City, UT, 2006. [Online]. Available: https://www.hydrogen.energy.gov/pdfs/progress06/ii_a_2_tao.pdf

[23] L. C. Juarez-Martinez, G. Espinosa-Paredes, A. Vazquez-Rodrigues and H. Romero-Paredes, "Energy optimization of a sulfur-iodine thermochemical nuclear hydrogen production cycle," *Nuclear Engineering and Technology,* vol. 53, pp. 2066–2073, 2021. [Online]. Available: https://doi.org/10.1016/j.net.2020.12.014

[24] J. P. O'Connell, P. Narkprasert and M. B. Gorensek, "Process model-free analysis for thermodynamic efficiencies of sulfur-iodine processes for thermochemical water decomposition," *International Journal of Hydrogen Energy,* vol. 34, pp. 4033–4040, 2009. [Online]. Available: https://doi.org/10.1016/j.ijhydene.2008.08.024

[25] M. Sakurai, H. Nakajima, K. Onuki, K. Ikenoya and S. Shimizu, "Preliminary process analysis for the closed cycle operation of the Idoine-Sulfer Thermochemical Hydrogen Production Process," *International Journal of Hydrogen Energy,* vol. 24, pp. 603–612, 1999. [Online]. Available: https://doi.org/10.1016/S0360-3199(98)00119-0

[26] Y. Chikazawa, T. Nakagiri, M. Konomura, S. Uchida and Y. Tsuchiyama, "A System Design Study of a Fast Breeder Reactor Hydrogen Production Plant Using Thermochehemical and Electrolytic Hybrid Process," *Nuclear Technology,* vol. 155, no. 3, pp. 340–349, 2006. [Online]. Available: https://doi.org/10.13182/NT06-A3766

[27] T. Nakagiri, S. Kato and K. Aoto, "Hydrogen production experiment by thermo-chemical and electrolytic hybrid hydrogen production process," in *16th World Hydrogen Energy Conference*, Lyon, France, 2006. [Online]. Available: https://www.osti.gov/etdeweb/biblio/20799315

[28] M. Rawool-Sullivan, P. D. Moskowits and L. N. Shelenkova, “Technical and proliferation-related aspects of the dismantlement of Russian-Alfa-Class nuclear submarines,” *The Nonproliferation Review,* vol. 9, no. 1, pp. 161–171. [Online]. Available: https://nonproliferation.org/research/nonproliferation-review/

[29] Gen-IV Forum, “Gen-IV International Forum,” 2020. [Online]. Available: https://www.gen-4.org/gif/jcms/c_44720/annual-reports. [Accessed 15 April 2022].

[30] “Nuclear-Power,” 11 August 2014. [Online]. Available: https://www.nuclear-power.com/breeder-reactor/. [Accessed 15 April 2022].

[31] C. E. Mandeville and C. P. Swann, “The Scattering of Fast Neutrons by Bismuth and Lead,” *Physics Review,* vol. 84, no. 2, pp. 214–217, 1951. [Online]. Available: https://journals.aps.org/pr/abstract/10.1103/PhysRev.84.214

[32] Fazio, Concetta, NEA Expert Group, Heavy Liquid Metal Technologies, *Handbook on Lead-bismuth Eutectic Alloy and Lead Properties*, *Materials Compatibility, Thermal-hydraulics and Technologies*, Nuclear Energy Agency, 2015. [Online] Available: https://inis.iaea.org/search/search.aspx?orig_q=RN:46133907

[33] C. F. Smith, “Heavy Liquid Metal (HLM) Cooled Fast Small Modular Reactors,” in *Encyclopedia of Nuclear Energy, vol. 1.* , Elsevier Inc, 2021, pp. 732–748. [Online]. Available: http://dx.doi.org/10.1016/B978-0-12-819725-7.00189-6

[34] L. A. Dawson, C. M. Mendez Cruz, M. D. Carlson, D. D. Fleming and G. E. Rochau, “Supercritical CO2-Brayton Cycle - Potential benefits, applications, technology development status and future plans,” Sandia National Laboratories, Albuquerque, New Mexico, 2016. [Online]. Available: https://www.osti.gov/servlets/purl/1378068

[35] K. Erdogan, P. G. Debenedetti and C. J. Peters, *Supercritical Fluids: Fundamentals and Applications*, Springer Science+Business Media, B.V., 2000. [Online]. Available: https://doi.org/10.1007/978-1-4615-2674-2_6

[36] P. Wu, G. Chuntian, S. Jianquing and S. Arkady, “Development and Verification of a Transient Analysis Tool for Reactor System Using Supercritical CO2 Brayton Cycle as Power Conversion System,” *Science and Technology of Nuclear Installations,* vol. 2018, p. 6801735, 2018. [Online]. Available: https://doi.org/10.1155/2018/6801736

[37] M. Marchionni, G. Bianchi and S. Tassou, “Review of supercritical carbon dioxide (sCO2) technologies for high-grade waste heat to power conversion,” *SN Applied Sciences,* vol. 2, no. 611, 2020. [Online]. Available: https://link.springer.com/article/10.1007/s42452-020-2116-6

[38] L. Cinotti, C. F. Smith and H. Sekimoto, “Lead-Cooled Fast Reactor (LFR) Overview and Perspectives,” in *Proceedings of the GIF Symposium*, Paris, France, 2009. [Online]. Available: https://www.osti.gov/biblio/1113427

[39] J. Sienicki, A. Moisseytsev, D. Wade and A. Nikiforova, “Status of Development of the Small Secure Transportable Autonomous Reactor (SSTAR) for Worldwide Sustainable Nuclear Energy Supply,” in *Proceedings of ICAPP*, Nice, France, 2007. [Online]. Available: https://www.osti.gov/biblio/932940

[40] A. Alemberti, V. Smirnov, C. F. Smith and M. Takahashi, “Overview of lead-cooled fast reactor activities,” *Progress in Nuclear Energy,* vol. 77, pp. 300–307, 2014. [Online]. Available: https://doi.org/10.1016/j.pnucene.2013.11.011

[41] G. J. Suppes and T. Storvick, “Production of Energy,” in *Sustainable Nuclear Power*, San Diego, CA, Elsevier Academic Press, 2006, pp. 185 - 200. [Online]. Available: ProQuest

[42] C. Lamy and P. Millet, “A critical review on the definition used to calculate the energy efficiency coefficients of water electrolysis cells working under near ambient temperature conditions,” *Journal of Power Sources,* vol. 447, p. 227350, 2020. [Online]. Available: https://doi.org/10.1016/j.jpowsour.2019.227350

[43] P. Wu, C. Gao, Y. Huang, D. Zhang and J. Shan, “Supercritical CO2 Brayton cycle design for Small Modular Reactor with a Thermodynamic Analysis Solver,” *Science and Technology of Nuclear Installations,* p. 5945718, 2020. [Online]. Available: https://doi.org/10.1155/2020/5945718

[44] Y. Zhang, M. Peng, G. Xia, G. Wang and C. Zhou, “Performance analysis of S-CO2 recompression Brayton cycle based on turbomachinery detailed design,” *Nuclear Engineering and Technology,* vol. 52, pp. 2107–2118, 2020. [Online]. Available: https://doi.org/10.1016/j.net.2020.02.016

[45] X. Yang and Z. Cai, “Thermodynamic performance analysis of Supercritical Carbon Dioxide Brayton cycle,” Dongguan Univerisity of Technology, Dongguan, China, 2020. [Online]. Available: http://dx.doi.org/10.2298/TSCI200314294Y

[46] C. Lamy, “From hydrogen production by water electrolysis to its utilization in a PEM fuel cell or in a SO fuel cell: Some consideration on the energy efficiencies,” *Journal of Hydrogen Energy,* vol. 41, no. 34, pp. 15415-15425, 2016. [Online]. Available: https://doi.org/10.1016/j.ijhydene.2016.04.173

[47] M. Santarelli, M. F. Torchio and P. Cochis, “Parameters estimation of a PEM fuel cell polarization curve and analysis of their behavior with temperature,” *Journal of Power Sources,* vol. 159, pp. 824–835, 2006. [Online]. Available: https://doi.org/10.1016/j.jpowsour.2005.11.099

[48] B. Lee, K. Park and H.-M. Kim, “Dynamic simulation of PEM water electrolysis and comparison with experiments,” *International Journal of Electrochemical Science,* vol. 8, pp. 235–248, 2013. [Online]. Available: http://www.electrochemsci.org/papers/vol8/80100235.pdf

[49] M. W. Chase, C. A. Davies, J. R. Downey, D. J. Frurip, R. McDonald and A. N. Syverud, “NIST-JANAF Thermochemical Tables,” 1985. [Online]. Available: https://janaf.nist.gov/. [Accessed 25 04 2022]

INITIAL DISTRIBUTION LIST

1. Defense Technical Information Center
   Ft. Belvoir, Virginia

2. Dudley Knox Library
   Naval Postgraduate School
   Monterey, California